Gomathi Ramachandran
Tamar Schlick*
The Howard Hughes Medical Institute and New York University Chemistry Department Courant Institute of Mathematical Sciences 251 Mercer Street New York, New York 10012, USA

Buckling Transitions in Superhelical DNA: Dependence on the Elastic Constants and DNA Size

Buckling transitions in superhelical DNA are sudden changes in shape that accompany a smooth variation in a key parameter, such as superhelical density. Here we explore the dependence of these transitions on the elastic constants for bending and twisting, A and C, important characteristics of DNA's bending and twisting persistence lengths. The large range we explore extends to other elastic materials with self-contact interactions, modeled here by a Debye–Hückel electrostatic potential.

Our collective description of DNA shapes and energies over a wide range of $\rho = A/C$ reveals a dramatic dependence of DNA shape and associated configurational transitions on ρ: transitions are sharp for large ρ but masked for small ρ. In particular, at small ρ, a nonplanar circular family emerges, in agreement with Jülicher's recent analytical predictions; a continuum of forms (and associated writhing numbers) is also observed.

The relevance of these buckling transitions to DNA in solution is examined through studies of size dependence and thermal effects. Buckling transitions smooth considerably as size increases, and this can be explained in part by the lower curvature in larger plasmids. This trend suggests that buckling transitions should not be detectable for isolated (i.e., unbound) DNA plasmids of biological interest, except possibly for very large ρ. Buckling phenomena would nonetheless be relevant for small DNA loops, particularly for higher values of ρ, and might have a role in regulatory mechanisms: a small change in superhelical stress could lead to a large configurational change.

Writhe distributions as a function of ρ, generated by Langevin dynamics simulations, reveal the importance of thermal fluctuations. Each distribution range (and multipeaked shape) can be interpreted by our buckling profiles. Significantly, the distributions for moderate to high superhelical densities are most sensitive to ρ, isolating different distribution patterns. If this effect could be captured experimentally for small plasmids by currently available imaging techniques, such results suggest a slightly different experimental procedure for estimating the torsional stiffness of supercoiled DNA than considered to date.
© 1997 John Wiley & Sons, Inc.

Received September 12, 1995; accepted December 15, 1995.

* To whom correspondence should be addressed.

Biopolymers, Vol. 41, 5–25 (1997)
© 1997 John Wiley & Sons, Inc.
CCC 0006-3525/97/010005-21

INTRODUCTION

Closed-circular DNA adopts a variety of higher order forms in which the DNA twists and bends about the global double-helical axis. These forms are known as supercoiled or superhelical DNA. Supercoiling condenses the DNA significantly and also stores energy that can be readily available for essential biological functions such as replication, recombination and transcription. This compact state also facilitates further packaging of DNA with proteins. Thus, DNA supercoils define an important functional state of the hereditary material. Understanding the structural response of DNA to superhelical stress is therefore a subject of great importance.

In closed-circular DNA systems, the closure of the ring determines the linking number of the DNA, Lk. This topological invariant is changed only by breaking one or two of the DNA strands. Lk describes the number of times that a DNA strand winds about the closed circular axis of the DNA (for a rigorous definition, see Ref. 1). In relaxed closed-circular DNA, Lk is directly related to the number of primary turns of the DNA: $Lk_0 = N/h$, where N is the number of base pairs (bp) and h is the number of bp per turn (about 10.5 for B-DNA). When superhelical stress is imposed, $Lk \neq Lk_0$, and the DNA is said to be underwound or overwound with respect to the relaxed state. This nonzero difference $\Delta Lk = Lk - Lk_0$, known as the *linking number difference,* is relieved by bending and twisting about the global double-helical axis, thereby partitioning ΔLk into twist and writhe: $\Delta Lk = Wr + \Delta Tw$.[1] In this fashion, interesting new geometrical states of DNA that are functionally important arise depending upon the amount of torsional stress.

The diversity of forms that supercoiled DNA assumes depends on many factors. These can be internal, such as the degree of torsional stress, and external, such as the concentration of salt in solution. Electron-microscopy images of supercoiled DNA reveal that supercoiled DNA is often wrapped about itself in an interwound (or plectoneme) configuration.[2] If the DNA is long enough, branches can result.[2] Other experiments [e.g., gel electrophoresis,[2] small angle x-ray scattering,[3] scanning force microscopy (SFM),[4,5] and cryo-electron microscopy[6]] can measure various properties that depend on the supercoiled form of DNA and therefore allow analysis of the shape and possibly fluctuations of DNA. However, since experimental resolution is limited, complementary theoretical modeling can provide insight into important structural and energetic aspects of supercoiled DNA. Systematic modeling can also help analyze and interpret the experimental observations.

One successful theoretical model of supercoiled DNA involves the Kirchhoff rod treatment based on elasticity theory and mechanics. Typical assumptions involve circular cross sections and homogeneous bending. Though it is well known that DNA exhibits preferential bending into major and minor grooves,[7] this assumption of uniform bending is reasonable for DNA that has no intrinsic curvature (i.e., is naturally straight). Still, several groups are developing models for intrinsically curved DNA within the elastic-rod formalism.[8,9]

Many investigators have explored the minimum energy configurations of the elastic-rod model for DNA by theoretical techniques. Hearst and Hunt modeled the DNA as an infinitely thin Kirchhoff elastic rod to study highly writhed states.[10,11] Later, Shi and Hearst[12] developed a new curvature-torsion coordinate framework to study DNA supercoiling on the basis of the nonlinear Schrödinger equation. Le Bret[13] and Benham[14] studied the first buckling transition, the abrupt change from the circle to the figure-8 interwound structure in the context of elasticity theory. In a later work,[15] Le Bret also suggested that higher order buckling transitions may occur. Recently, Jülicher[16] presented a detailed phase diagram (spanning ΔLk values from 0 to 3) for supercoiled DNA by analytically approximating the equilibrium profiles of a homogeneous elastic rod model. Different DNA families were studied (circles, nonplanar circles, figure-8 structures, and interwounds), with transitions among them examined and stability issues discussed. Other recent analytical works focus on the role of thermal fluctuations and entropic effects.[17,18]

A variety of computer simulations have also been developed and applied to obtain minima as a function of important parameters. These include simulated annealing,[19,20] Newton minimization,[21,22,23] and finite-element analyses (FEA).[24,25] In addition to these minimization studies, statistical and kinetic models have also been developed. Monte Carlo approaches provide collective descriptions of configuration space (e.g., Ref. 26). More recent dynamic approaches by molecular dynamics,[27] Langevin dynamics,[21,22,28] Brownian dynamics,[29] and those based on the dynamic theory of elastic rods[9,30] are providing complementary information on the kinetic aspects of supercoiled DNA (e.g., writhe relaxation, folding,

diffusion). For a recent review of these exciting developments, see Ref. 31.

While our major interest lies in dynamic simulations of supercoiled DNA, we became interested in buckling catastrophes that emerged from FEA and our deterministic minimization study.[24,32] These abrupt structural changes in global shape are of interest for several reasons. First, they are intrinsic to the elastic rod model[33] applied to DNA and hence important. Second, they may be biologically relevant, for example, as signals to enzymes that regulate DNA by binding and altering Lk.[34,35] Even if thermal fluctuations for long DNA mask the sudden configurational changes expected theoretically from the elastic model, buckling transitions may be important for small looped segments of DNA. Third, buckling transitions are sensitive to the elastic constants A and C for bending and torsional rigidity, respectively; since there is significant uncertainty in the appropriate value of C for superhelical DNA, results as a function of $\rho = A/C$ might provide a slightly different direction for comparing theoretical results with experiment to estimate the torsional stiffness.

In this paper, we present a systematic description of the expected DNA configurations (families) over a wide range of ρ values. The resulting profiles clarify the dependence of supercoiling on the ratio A/C. Such relationships were examined in part in prior studies but not with realistic nonbonded potentials for DNA.[13,14,16] Our potential energy includes both elastic and electrostatic contributions, the latter in Debye-Hückel form.[22] All terms are adapted for a macroscopic treatment. Both energy minimization and Langevin dynamics simulations are used to determine the writhe and energy profiles and to examine them in light of thermal fluctuations. The relevance of these transitions to long DNA (thousands of bp) is also examined. We find that thermal effects mask these transitions, except for very large ρ values. Finally, we suggest how the data might be used with experiment to estimate C and explore the size and system dependence of C.

In the following section we present the details of our model and the methods used. In the third section, we present and discuss minimization profiles as a function of ΔLk: we consider four different values of ρ for closed-circular DNA systems of 1000 bp. Next, variations with size are examined by comparing results for DNA systems of 1000 and 2000 bp. Finally, distributions of writhe as a function of ρ and ΔLk are also presented, as obtained from Langevin dynamics simulations, to evaluate the role of thermal fluctuations. The last section summarizes and discusses these findings and suggests possible applications.

NUMERICAL MODEL AND SIMULATION DETAILS

Energy Model

We use the B-spline model to represent the DNA duplex curve in terms of a small number of control points[21] (e.g., 14 per 1000 bp). From these control points we generate curve points (e.g., 8 or 16 per spline segment), which are then used for energy evaluation. The potential energy E consists of elastic and electrostatic components. The elastic terms include homogeneous bending (E_B) and twisting (E_T) potentials. The Coulombic term (E_C) is in Debye-Hückel form and considers pairwise interactions among charged linear segments along the DNA curve. A simple harmonic term (E_L) is also included as a computational device to ensure that the total chain length L remains very close to its target value L_0. The energy components are given as follows:

$$E_B = \frac{A}{2}\oint \kappa^2(s)\,ds \tag{1}$$

$$E_T = \frac{2\pi^2 C}{L_0}(\Delta Lk - Wr)^2 \tag{2}$$

$$E_L = K(L - L_0)^2 \tag{3}$$

$$E_C = B(\beta)\int\int \frac{e^{-\beta r_{ij}}\,dl_i\,dl_j}{r_{ij}} \tag{4}$$

In these expressions, s denotes arc length, κ denotes curvature, and the integrals are evaluated over the total length of the curve. The parameter K is a stiffness constant chosen for computational reasons (i.e., not physical stretching, which might be a future addition). The writhing number Wr is a geometric descriptor of shape.[1] In the electrostatic potential, β is the Debye-Hückel screening parameter ($0.33\sqrt{c_s}$ at room temperature, where c_s is the molar salt concentration)[22]; $B(\beta)$ is a salt-dependent coefficient[22]; r_{ij} is the distance between points i and j along the DNA chain; and l_i denotes the length of each charged segment along the chain. Full details of the electrostatic treatment are given in Ref. 22, and details of the B-spline model and the elastic-energy functions are given in Ref. 21.

Systems and Parameters

We use closed circular DNA systems of 1000 and 2000 bp to generate energy minimization profiles

and 1000 bp for configurational distributions. The Langevin dynamics simulations are started at an equilibrium configuration at the temperature T = 300 K. A salt concentration of 1.0 M is used in all these studies. This is because profiles are more interesting at this value than at 0.1 M due to a larger range of Wr observed over the same superhelical density range.[22] At 1.0 M salt, E_C is much smaller (by an order of magnitude) than at lower salt since repulsive interactions between the polyelectrolyte backbone are more effectively screened.[22] However, profiles (and energies) shift consistently at lower salt,[22] reducing the numerical values of Wr but not changing the curve shapes. Furthermore, the position of the first buckling transition appears to be dominated by the ratio of A/C and not affected significantly by the salt concentration.[22]

Algorithms

To find potential-energy minimized structures we use the truncated-Newton scheme.[36] For dynamics trajectories, we use a Langevin dynamics protocol with the damping constant $\gamma = 9.77 \times 10^{10}$ s^{-1} (program units), as calibrated in Ref. 28 to give both an approximate representation of solvent damping and optimal configurational sampling. The Langevin equation of motion is integrated numerically by the Langevin/implicit-Euler (LI) algorithm with a timestep $\tau \simeq 100$ fs in program units.[37] We have shown that the LI algorithm agrees well with the Verlet algorithm (with a program time step of $\simeq 5$ fs) at this value of γ,[38] and moreover, provides a computational advantage of about a factor of three. The program timestep of 100 fs corresponds to an effective physical time step of approximately $\sim$ 10 ns,[38] since both the masses and the value of γ are scaled for computational reasons.

Full details concerning the algorithms are given in Refs. 36, 37, and 39. The calibration of the timestep is described separately in Ref. 38, a work that extends Ref. 40. Extensions of the dynamic model to Brownian dynamics with hydrodynamics are described separately (G. Ramachandran and T. Schlick, in preparation).

Elastic Constants

Currently, there is a wide range of possible values for C, from 1.5 to 4×10^{-19} erg cm. In contrast, an average value for the bending constant A has been more narrowly bracketed to correspond to a bending persistence length, p_b, of around 55 nm at moderate salt, yielding the value $A = 2.3 \times 10^{-19}$ erg cm ($A = k_B T p_b$, where k_B is Boltzmann's constant). Still, over the large sodium ion concentration range of 0.001–1.0 M, a broad range for p_b of 28–100 nm is noted,[41] corresponding to A between 1.12 and 4.02×10^{-19} erg cm. In any case, the uncertainty in C leaves a large possible range for $\rho = A/C$, both greater than and lower than unity. (See Ref. 31 for a discussion on the relation to the Poisson ratio.)

Early analyses of fluorescence depolarization of DNA by Barkley and Zimm[42] suggested the broad range for C from 1×10^{-19} to 4×10^{-19} erg cm. Shore and Baldwin's measurements of chain cyclization[43,44] suggested a torsional constant of $C = 2.4 \times 10^{-19}$ erg cm. Measurements based on gel shifts analyzed by Horowitz and Wang[45] pointed to a value of $C = 2.9 \times 10^{-19}$ erg cm as a lower limit. A similar value of C (around 3×10^{-19} erg cm) was obtained[46] by a numerical treatment based on writhe distributions and experimentally based ΔLk variances. This procedure was suggested by Benham,[47] developed by Volgodskii et al.,[48] and refined to include excluded-volume effects by Klenin et al.[46]

These values for DNA's torsional stiffness are somewhat higher than estimates based on time-resolved fluorescence and dynamic light scattering,[49,50] about $C = 2 \times 10^{-19}$ erg cm. Values in this range were also suggested by earlier fluorescence depolarization measurements of Millar et al.[51] ($C = 1.43 \times 10^{-19}$ erg cm). More recent analyses based on static base-sequence variations in B-DNA crystal structures[52,53] also point to a lower C value ($C = 1.4 \times 10^{-19}$ erg cm), which corresponds to observed rms twist fluctuations of 5.9° in the x-ray data.

From the estimates given above for the torsional stiffness of the DNA, by taking $A = 2.3 \times 10^{-19}$ erg cm as the effective bending constant at 0.1 M sodium, we see that ρ might span the range 0.5–2.3. Variations in ρ are also expected with chemical changes in the environment, e.g., alcohol-induced B to A-DNA transitions. Considering the sensitivity of both analytical and numerical results to ρ, it is valuable to explore how this ratio might affect supercoiled DNA in the context of a simple model.

Ratio of the Elastic Constants in the Context of an Electrostatic Treatment

A point that requires clarification in our study is the meaning of ρ in the context of a model that includes an explicit electrostatic potential in addition to elastic bending and twisting terms. In this case, bending persistence length contributions come from two sources: the bending term and the electrostatic potential. The latter contributes due

to the repulsive interactions from incompletely screened backbone charges. Therefore, when comparing results to experiment, the *persistence* lengths for bending and twisting are the relevant quantities to consider, not the ρ value per se.

The *effective* persistence length in the context of an elastic plus electrostatic model and its dependence on the input A is a complex subject on its own (Jian, H., Ramachandran, G., Schlick, T., & Vologodskii, A., work in progress). Such studies are best done for short linear DNA and must consider carefully excluded volume effects. However, it is clear that the added electrostatic term *increases* the effective persistence length from that corresponding to the bending stiffness alone (i.e., A/k_BT). The percentage of increase depends on the value of A used. Furthermore, a much wider increase is realized in the range of low sodium salt concentration (e.g., 0.01–0.1M), in comparison to the range 0.1–1.0M. This is consistent with what emerges from many experimental studies[41] but not all.[54] Thus, in terms of parameterizing a numerical model, the chosen A can have a substantial range to correspond to any target experimental value.

In our work, we use $A = 1.28 \times 10^{-19}$ erg cm, corresponding to the nonelectrostatic contribution to the persistence length of approximately 31 nm[54] and a sodium-ion concentration of 1.0M. Alternatively, a higher value of about 2×10^{-19} erg cm has been used in the context of a Debye–Hückel treatment.[55] Through rough comparisons of writhe distributions for nicked DNA we found an effective increase in the persistence length of about 33% in our Debye–Hückel treatment with respect to an elastic model (with an excluded volume term in the form of Lennard-Jones[21]) where A was varied for calibration. For reference, when we set A to 2.3×10^{-19} erg cm in our elastic plus electrostatic model the increase was smaller, about 26%. Therefore, we can very roughly consider the increase of persistence length in our electrostatic model with $A = 1.28 \times 10^{-19}$ erg cm to be about 33% corresponding instead to $A = 1.7 \times 10^{-19}$ erg cm in an electrostatic-free model. This implies, for example, that the ratio $\rho = 1$ as used in our model ($A = C = 1.28 \times 10^{-19}$ erg cm) corresponds to $\rho' = 1.7/1.28 = 1.33 = 1.33\rho$ (see Table I).

Computational Performance

All computations are performed on a Silicon Graphics Indigo 2 Extreme workstation with a 150 MHz IP22 processor. Minimizations for the DNA circles of 1000 bp require from 2 seconds to 20 minutes, depending on the starting structure. An MD simulation of 10,000 iterations (roughly 100 μs in physical time[38]) takes approximately 3 central processing unit hours for 1000 bp.

RESULTS

Presentation as DNA Profiles

In the work described below we fix $A = 1.28 \times 10^{-19}$ erg cm and change the value of C to study different A/C values. We consider four values of ρ—3, 1, 0.71, and 0.43—for the following reasons. The values 0.43, 0.71, and 1 lie within the biologically relevant range for DNA.[31] In particular, the first two values correspond in our formulation (see discussion above on elastic constants) to the commonly used values of $C = 3$ and 1.8×10^{-19} erg cm,[45,56] respectively (see Table I). We have also used the particular value of $\rho = 0.71$ recently.[31] The value $\rho = 3$ clearly lies outside of the experimentally expected range for DNA, but is useful here for extensive interpretation of our results and possibly for other elastic materials. (Note that by pure application of elasticity theory, $1 \leq \rho \leq 1.5$,[31] but de-

Table I Elastic Constants and Related Quantities for DNA[a]

ρ (This Work)	ρ'	ρ''	C ($\times 10^{-19}$ erg cm)	$\langle\theta_i^2\rangle^{1/2}$
3	4.0	5.40	0.43	10.3°
1	1.33	1.80	1.28	5.9°
0.71	0.94	1.28	1.80	5.0°
0.43	0.57	0.77	3.00	3.9°

[a] The column headings are defined as follows: ρ is the ratio of the elastic constants (A/C) as used in this work with $A = 1.28 \times 10^{-19}$ erg cm corresponding to the nonelectrostatic contribution to the bending persistence length (see text); ρ' is the associated A/C ratio if the effective A were 1.7×10^{-19} erg cm (as estimated, see text); ρ'' is the associated A/C if A is equal to 2.3×10^{-19} erg cm corresponding to the effective persistence length at moderate salt (see text); C is the torsional-rigidity constant; and $\langle\theta_i^2\rangle^{1/2}$ is the rms twist angle. The rms bending deviations, $\langle\theta_b^2\rangle^{1/2} = \sqrt{2(k_BT)d/A}$, where $d = 0.34$ nm is the distance between base pairs, are 8.4°, 7.3°, and 6.2° corresponding to $A = 1.28$, 1.7, and 2.3×10^{-19} erg cm, respectively. The rms twist angle is given as a function of C by $\langle\theta_t^2\rangle^{1/2} = \sqrt{k_BTd/C}$.

viations are expected for real DNA, a nonuniform material with noncircular cross section, where bending is asymmetric and twisting is sequence dependent.)

Figures 1–4 display profiles obtained by energy minimization of closed-circular DNA of length 1000 bp for our four ρ values. Figure 5 shows corresponding views for a system of 2000 bp with $\rho = 0.71$. The five parts of each figure show: the magnitude of the writhing number (part a), the total energy E (part b), the twist energy E_T (part c), the bending energy E_B (part d), and the Coulombic energy E_C (part e), all as a function of ΔLk. We use ΔLk in the range 0 to -7 and hence obtain negative values for Wr. (For display, we plot $-Wr$ vs $-\Delta Lk$). Representative configurations for some families are also shown. These profiles are constructed by performing a large number of minimizations from a wide range of starting points, such as the circle, the figure-8 interwound structure, and other interwounds obtained by minimization. See Ref. 32 for further details.

We use different symbols to distinguish among related supercoil forms such as the circle ($F0$), the figure-8 interwound ($F1$), the interwound with $|Wr| \simeq 2(F2)$, and so on.[32] Families that are not part of the global minimum energy are shown by dashed lines. The various families are most easily distinguished according to the twist and Coulombic energy components (see Figure 1c and 3e for example); we use the criterion of a sharp drop in E_T to detect another configurational family. For some configurational families, especially the highly writhed and bent forms, there is a discontinuity in the Coulombic energy *within* the family (see Figure 2e and 4e). This occurs even when there is a smooth transition in Wr between forms within a family. For example, in the $F3^+$ family at $\rho = 0.43$ (Figure 4a) there is a transition between bent interwounds and straight, more highly writhed, interwounds (see the two forms shown for the $F3^+$ family in Figure 4a and compare to Figure 4e).

Note from the Wr plots that more than one structure can exist at a given value of ΔLk. The corresponding crossing of associated energy curves (part b) shows when one family becomes energetically favored. In Figure 1b, for example, both $F1$ and $F2$ configurations are detected as minima for $4 < |\Delta Lk| < 5.2$. $F2$ is energetically favored for $|\Delta Lk| > 4.5$. $F1$ configurations are energetically favored over $F0$ for $|\Delta Lk| > 3.75$. These buckling transitions occur at large $|\Delta Lk|$ in comparison to those associated with the lower ρ values (e.g., 1, 1.5) typically used.[32] The dashed lines associated with higher energy forms often correspond to bent interwound forms (see, for example, the images corresponding to the higher energy families in Figure 2a).

Overall Sensitivity of Profiles to ρ

The strong sensitivity of the profiles to $\rho = A/C$ is apparent from the views. The extreme cases of $\rho = 3$ and $\rho = 0.43$ (Figures 1 and 4) show the most dramatic differences, but a systematic change as ρ is decreased is evident over this large range of ρ that we explore. Namely, we see that as ρ is decreased: (1) the Wr profiles smooth out (i.e., gaps in Wr among families become smaller); (2) the slope of $|Wr|$ vs $|\Delta Lk|$ curves (if one draws a coarse line) increases, though in a complex way (see below); and (3) the profiles generally become more intricate overall, i.e., more families that are close in energy and cannot be easily distinguished emerge at lower ρ. (In this connection, the $\rho = 1$ case may be special.)

For example, a gap of approximately one unit in Wr separates both the $F0$ and $F1$ families and the $F1$ and $F2$ families for $\rho = 3$ (Figure 1a). This implies that neither imperfect circles nor structures with $1.2 < |Wr| < 1.8$ are detected as minima for these ρ. These forms are unfavored due to the high cost of bending. When $\rho = 1$, a large unit gap still separates the writhe associated with the $F0$ and $F1$ forms (Figure 2a), but the second gap—notable for $\rho = 3$—has disappeared; instead, the figure-8 related forms realize a much broader range of writhe, and $|Wr|$ increases more steeply with $|\Delta Lk|$. For our smallest ρ value, 0.43 (Figure 4a), the first buckling catastrophe disappears altogether and a new family of imperfect circles emerges (Figure 6). Indeed, this result is expected from elasticity theory, and Jülicher predicted that these nonplanar rings become stable equilibria for $\rho < 0.61$.[16] Note that this family of nonplanar circles is energetically equivalent to the circle at about $|\Delta Lk| = 0.8$ and then becomes energetically equivalent to the figure-8 interwound forms at roughly $|\Delta Lk| = 1$. The $\rho = 0.43$ profile clearly shows that the families are merged more smoothly to one another at low values of ρ and that hardly any significant writhe jumps are present.

Sensitivity of Profiles to DNA Size

By comparing the two profiles corresponding to $\rho = 0.71$ for DNA systems of 1000 and 2000 bp (Figure 3 vs. 5), we clearly see how much simpler the latter profile is: Families beyond $F1$ are nearly indistinguishable for the larger DNA. For this rea-

son, we denote these configurations collectively by FN. Only the twist energy for the latter (Figure 5c) reveals nonsmooth behavior beyond $|\Delta Lk| = 2$, with pronounced drops near $|\Delta Lk| = 2, 4$, and 5.6. These first two $|\Delta Lk|$ values roughly correspond to emergence of $F2$ and $F3$ families for the system of 1000 bp (Figure 3a,c), but for the third we have no analogue. Possibly, a sudden change in curvature for the larger DNA is responsible for this pattern in the bending energy (see below). Overall, the smaller curvature in segments of the larger plasmid explain the smoother profiles.

Another observation concerns the $|\Delta Lk|$ value where buckling from the circle to the figure-8 interwound occurs. The critical value $|\Delta Lk_c|$, where the energies of the two forms are equivalent, is about 1.3 for both 1000 and 2000 bp at this ρ. Indeed, independence from length is expected from theory. (Note that we plot $-Wr$ vs $-\Delta Lk$ rather than the superhelical density, $\sigma = \Delta Lk/Lk_0$, in Figure 3a and 5a). The slope of the writhe curve is also steeper for 2000 bp than for 1000 bp.

These results clearly show that buckling behavior is sensitive to DNA length and thus buckling catastrophes are not expected for plasmids of biological interest (e.g., pBR322 is 4361 bp long). Our studies show that transitions may be relevant only for large ρ and/or small DNA systems. DNA loops, for example, might exhibit such phenomena, which may be related to biological regulation. A buckling transition for a DNA minicircle (178 bp) has indeed been observed experimentally.[57] We will address the related question of the effect of thermal fluctuations on these buckling phenomena in a separate subsection.

Analysis of Buckling in Terms of Curvature

A buckling catastrophe results when the DNA cannot accommodate a small change in $|\Delta Lk|$ by a small change in bending (curvature) and writhe. We saw that buckling behavior is sensitive to both ρ and DNA size. To further examine this sensitivity, we analyze in Figure 7 the curvature distribution along the DNA configuration for three values of ρ (3, 1, and 0.43) for two configurational families: $F1$ and $F2$. A similar distribution for $\rho = 0.71$ comparing systems of 1000 and 2000 bp is shown in Figure 8. In each panel of the figure, we show two curvature (the variable κ in Equation 1) curves superimposed, corresponding to the first and last structure of the $F1$ (or $F2$) family analyzed. The color configurations shown alongside the plot represent the two corresponding forms, whose color coding matches the points on the curve. For these presentations, we use discretizations involving 112 curve points for 1000 bp and 160 points for 2000 bp. Note that the small, jagged peaks arise from the discontinuity of the curvature function in terms of the control points. For the 1000 bp plots (Figures 7 and 8), 14 jagged peaks corresponding to 14 control points can be seen, and for 2000 bp (Figure 8), 20 peaks (20 control points) are evident.

From Figure 7 we see the natural characteristics of the figure-8 curvature distribution most clearly from the $\rho = 3$ panel: two minima and two broad maxima. Curvature is smallest at the straighter segments and largest at the apices of the bent structure. This "signature" of the figure-8 curvature does not change significantly as ρ is varied, though greater variations *within* the $F1$ family are noticeable as ρ is lowered (each of the two minima regions changes into two minima separated by a higher curvature region; this indicates a movement toward the $F2$ family). For the $F2$ interwound family, four minima, two major maxima, and two minor maxima can be identified. Greater diversity within the family members again emerges as ρ is lowered. This explains the "softer" buckling behavior noted for lower ρ values.

FIGURE 1 Energy-minimized profiles for closed circular DNA of length 1000 base pairs, $\rho = 3$. The energy includes bending, twisting, and Debye-Hückel potentials, as described in the text. The bending constant $A = 1.28 \times 10^{-19}$ erg cm is used (corresponding to the nonelectrostatic contribution to the persistence length), and the torsional rigidity constant C is varied to establish the desired ρ (i.e., $C = A/\rho$). The salt concentration is set in all cases to $1.0M$ sodium ions. (A lower salt concentration shifts the writhing numbers consistently.) Shown as a function of $-\Delta Lk$ are as follows: (a) The negative of the writhing number ($-Wr$), (b) the corresponding total energy E (in kcal/mol), (c) the twisting energy E_T, (d) the bending energy E_B, and (e) the Coulombic energy E_C. The various families ($F0$, $F1$, and $F2$) are distinguished by different symbols (see text), and dashed lines rather than symbols are used for configurational families that are not part of the global energy minimum. The $F0$ (circle) family has been followed until the circle is no longer found as a minimum when starting optimization from the circle. In (a), selected DNA configurations are also shown.

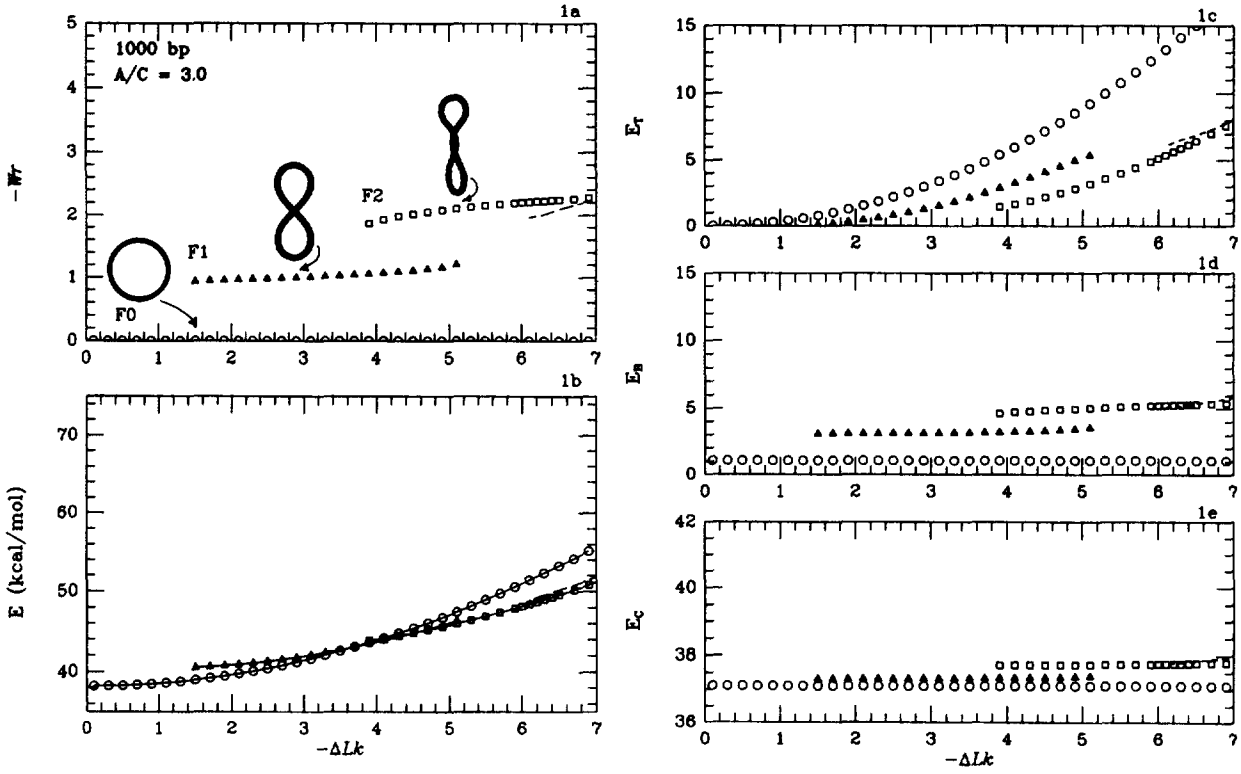

FIGURE 1

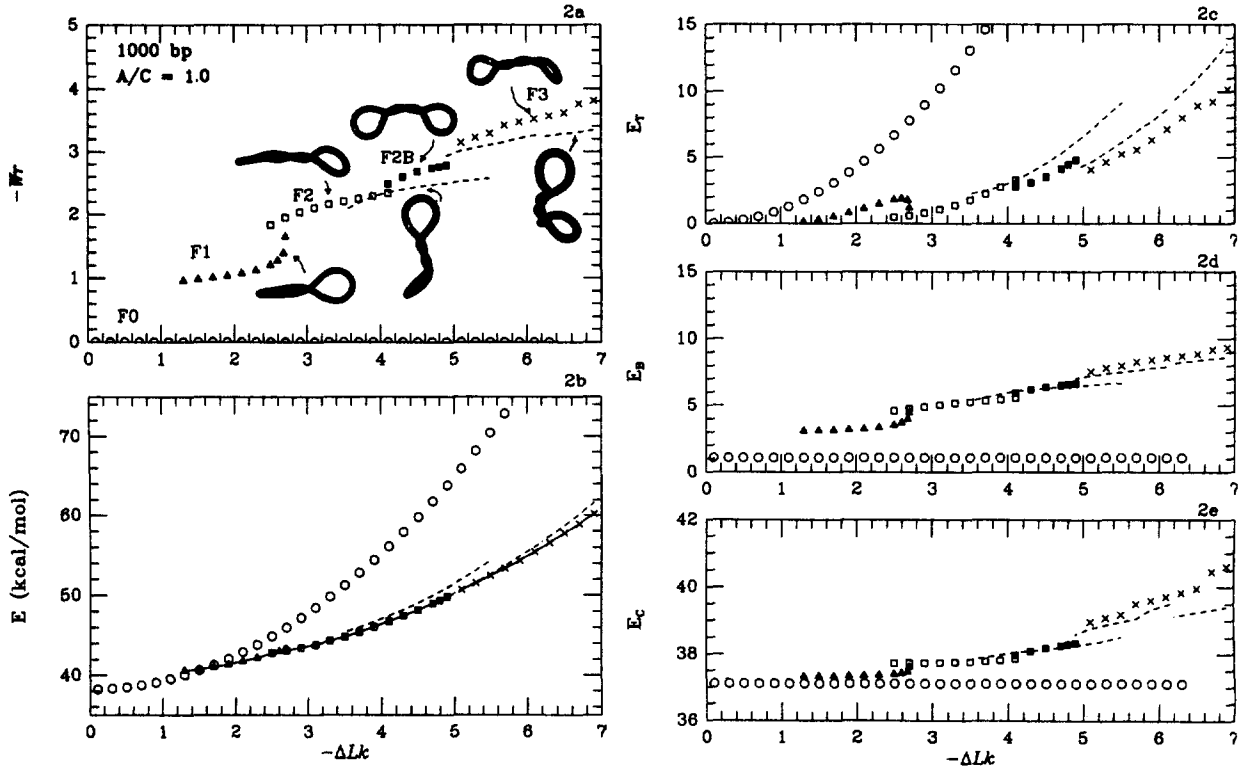

FIGURE 2 Energy-minimized profiles for closed circular DNA of length 1000 base pairs, $\rho = 1$. See Figure 1 caption.

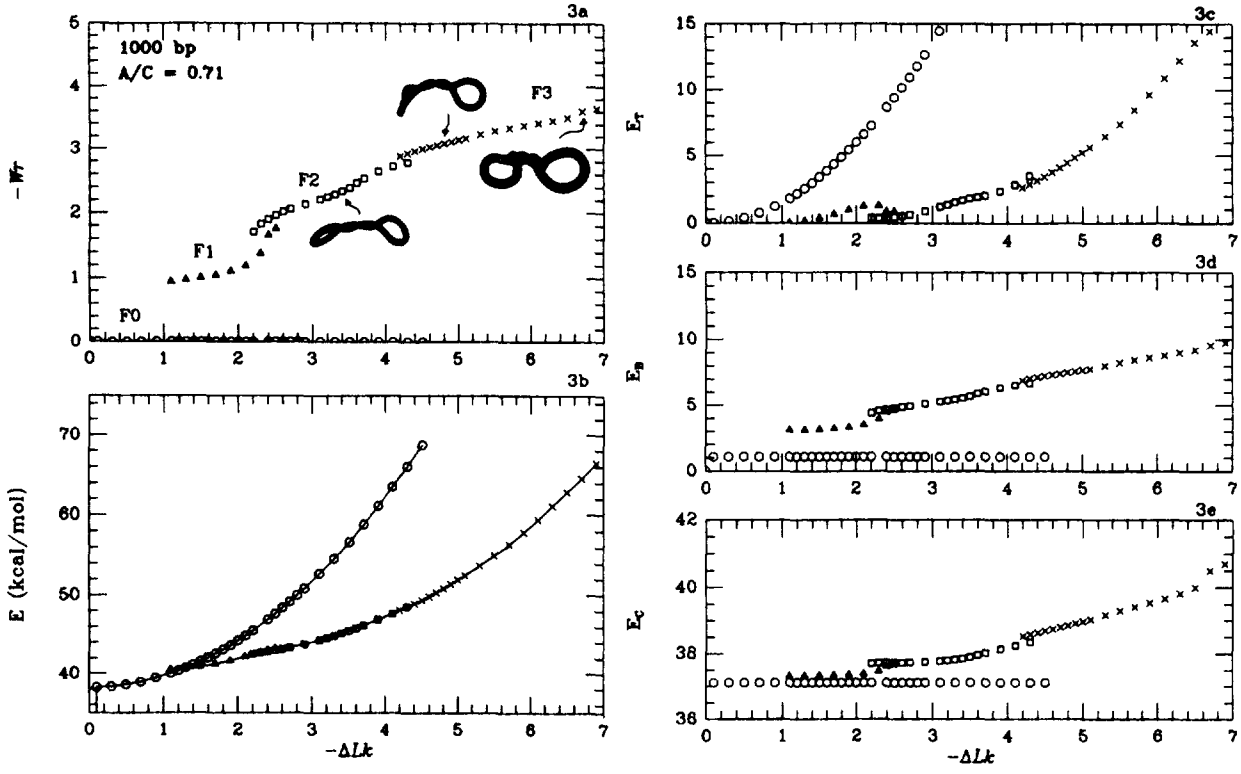

FIGURE 3 Energy-minimized profiles for closed circular DNA of length 1000 base pairs, $\rho = 0.71$. See Figure 1 caption.

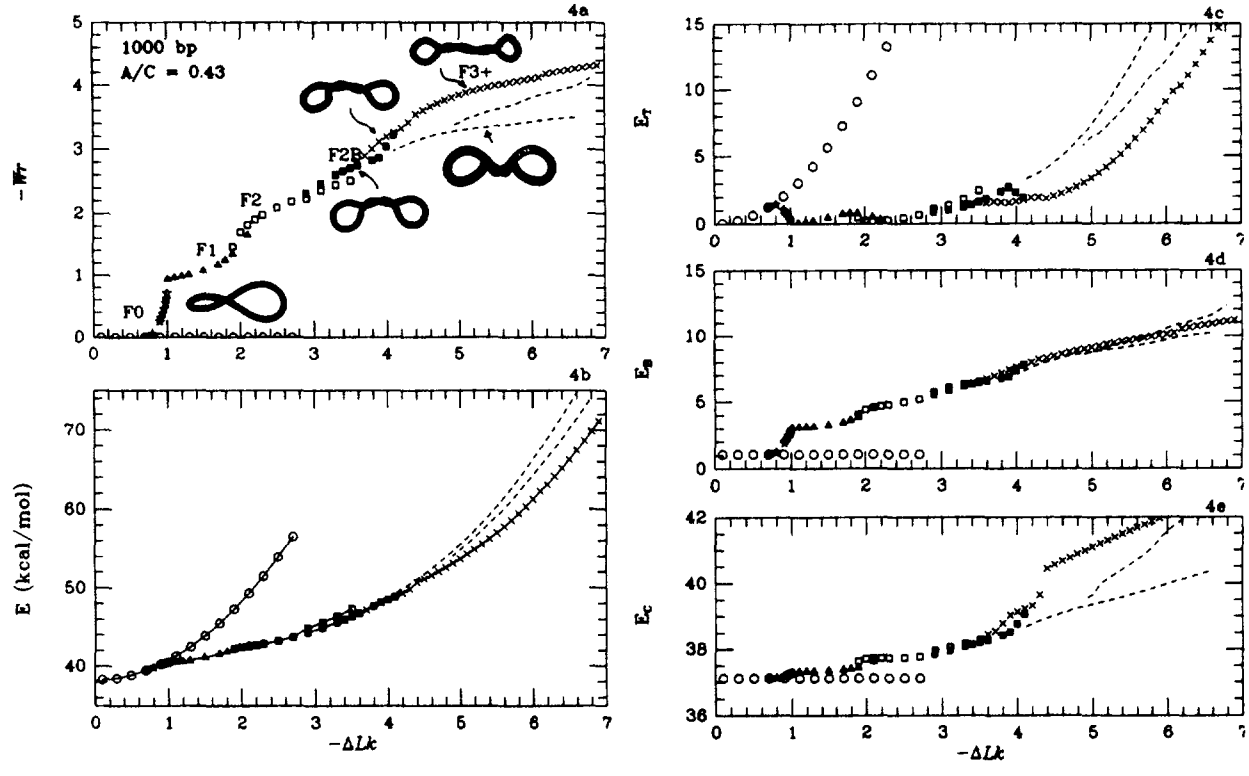

FIGURE 4 Energy-minimized profiles for closed circular DNA of length 1000 base pairs, $\rho = 0.43$. See Figure 1 caption.

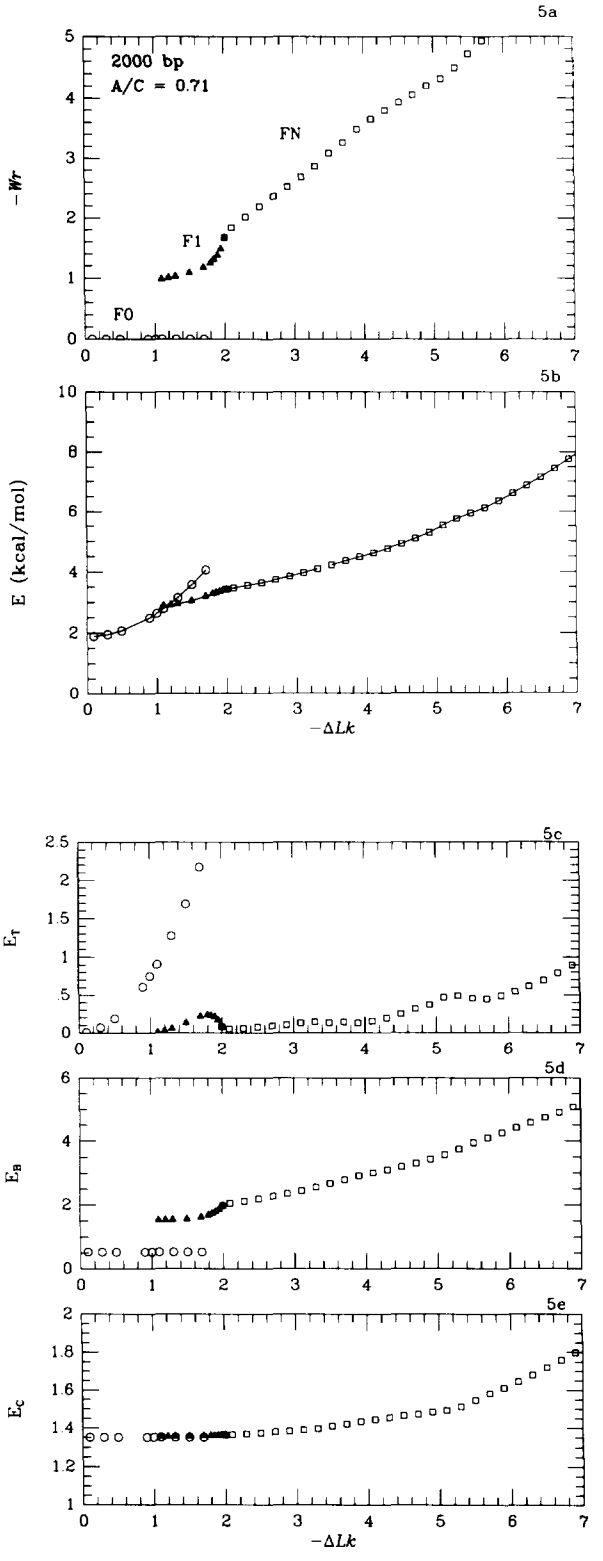

FIGURE 5 Energy-minimized profiles for closed circular DNA of length 2000 base pairs, $\rho = 0.71$. See Figure 1 caption. Note that there are no notable writhe jumps to distinguish the configurations beyond the $F1$ family. Thus, all structures outside of the $F1$ family are designated by FN.

Now, the smoother profiles for larger DNA systems can also be understood in terms of the curvature plots in Figure 8. For 2000 bp, the curvature *variations* along the DNA curve are much smaller compared to those associated with 1000 bp. The *magnitude* of curvature is also smaller in comparison to the smaller systems and hence E_B is lower for 2000 bp (about one half) for the same $|\Delta Lk|$. This fraction of one half remains when we increase the mesh size for our B-spline representation of the system of 2000 bp, so as to generate 240 curve points (data not shown), and is expected from the form of E_B [Eq. (1)].

Clearly, since curvature of a segment is inversely proportional to the radius of the circle associated with it, curvature is smaller for longer DNA. Thus, as $|\Delta Lk|$ is varied, continuous changes in curvature can be sustained at a lower energetic cost and thus buckling catastrophes are more easily masked for longer plasmids.

Buckling Analysis

The behavior of the $F1$ family (figure-8 forms) as a function of $|\Delta Lk|$ is particularly sensitive to ρ; hence, analysis of this behavior explains the more general buckling trends noted above. At $\rho = 3$, the writhe curve of the $F1$ family (Figure 1a) is roughly a straight line with a near-zero slope, and this family extends over nearly four units of $|\Delta Lk|$. Bending the DNA is energetically more expensive than twisting it, and thus nearly planar forms (with one or two crossings) are preferred over bent structures. When $\rho = 1$ (Figure 2a), the writhe of the $F1$ curve assumes a parabolic shape over a much smaller range of $|\Delta Lk|$ (about 1.4). The value $|Wr|$ rises slowly as $|\Delta Lk|$ is increased from 1.3 to 2.3, but then rises steeply. Similar parabolic patterns are seen for $\rho = 1$ and $\rho = 0.43$, though the lowest $|\Delta Lk|$ where a figure-8 form is identified (beginning of the family) decreases with ρ, and the ΔLk range associated with the family varies with ρ.

Examination of the bending and twisting energy curves clarifies these trends. For example, from Figure 1c,d we see that E_T rises monotonically with $|\Delta Lk|$ for $F1$, while E_B hardly changes, mirroring the Wr pattern. That is, the same bending (curvature) can be sustained more easily when ρ is large since E_T increases more slowly with $|\Delta Lk|$. As ρ is decreased, the twist penalty is greater—note the gradual increase in slope of the E_T curve for $F0$ as ρ is decreased. Thus, more families and larger variations in Wr (over the same $|\Delta Lk|$ range) are seen as ρ is decreased. Note the small structural differences among members of the $F1$ family for $\rho = 3$

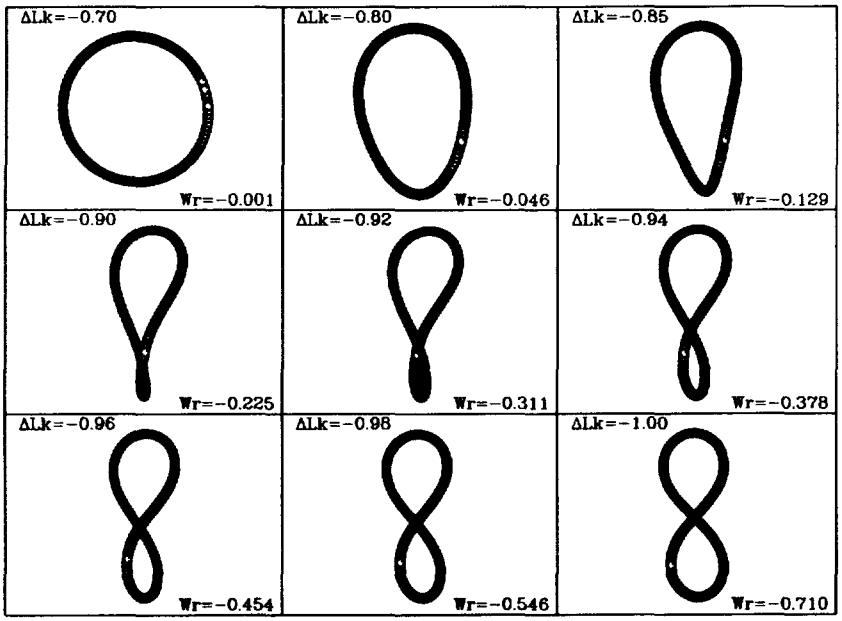

FIGURE 6 The nonplanar-circle family identified at $\rho = 0.43$. These forms correspond to the branch of $0 < |Wr| < 1$ shown in Figure 4a by open star symbols. Note the progression from a slightly bent circle at $-\Delta Lk = 0.7$ to the nearly figure-8 form at $-\Delta Lk = 1.0$.

(Figure 1a) in contrast to the large variations noted in $F1$ when $\rho = 0.43$ (Figure 4a).

In particular, the circle to figure-8 buckling transition occurs at lower $|\Delta Lk|$ as ρ is decreased since the critical $|\Delta Lk|$ where the lower curvature (of the circle) is competitive with twist-energy penalty involved (lower $|Wr|$ forms) decreases with ρ. In Figure 9 we show the critical $|\Delta Lk|$ value, $|\Delta Lk_c|$, where the energy of the circle is equal to that of the figure-8 form, as a function of ρ. The change is dramatic over the range of ρ explored here: $|\Delta Lk_c| = 3.7$, 1.6, 1.3, and 1.0, for $\rho = 3$, 1, 0.71, and 0.43, respectively (the point for $\rho = 1.5$, $|\Delta Lk_c| = 2.1$, is taken from Ref. 22). The linear dependence of ΔLk_c on ρ can be understood by equating the potential energies for the circle and the figure-8 structures and using $|Wr| = 0$ and 1, respectively, for these structures to evaluate the twist energy [Eq. (2)]. One then obtains the relation

$$\Delta Lk_c(\rho) = (\epsilon_B + \epsilon_c)\rho + 0.5 \qquad (5)$$

where the *terms* (not actual energies) involving bending and electrostatic energy differences between the circle and figure-8 (ϵ_B, ϵ_c) forms are independent of ρ and C:

$$\epsilon_B = \left(\frac{L_0}{4\pi^2 A}\right)\frac{A}{2}\left[\oint_{F1} \kappa^2(s)\,ds - \oint_{F0} \kappa^2(s)\,ds\right] \qquad (6)$$

$$\epsilon_c = \left(\frac{L_0}{4\pi^2 A}\right)[E_{c_{F1}} - E_{c_{F0}}] \qquad (7)$$

For our model, we obtain the constants $\epsilon_B = 0.9706$, $\epsilon_c = 0.0985$ (both quantities are dimensionless). Note also from Figure 9 that the "stability" line, $\sqrt{3}\rho$,[13,14,33] has a greater slope and crosses the $|\Delta Lk_c|$ line. For values of ρ beyond 0.8 (where the two lines cross) this implies that exchange of stability will occur for $|\Delta Lk| > |\Delta Lk_c|$, as expected. However, the stability line $\sqrt{3}\rho$ is most likely valid only beyond some critical ρ value.[16]

Buckling in View of Thermal Fluctuations

A central question in our application of an elastic treatment to DNA is the biological relevance of these buckling transitions. We already noted that buckling transitions are expected for DNA minicircles and loops, and that these phenomena may be related to protein-regulated events.[34,35] Furthermore, the higher ρ is, the more pronounced the buckling behavior will be. Can we offer additional quantitative data on buckling in view of thermal fluctuations for DNA in solution?

Interactions between the DNA and solvent molecules at ambient temperatures produce significant thermal motions.[58] Inertial forces become smaller (in comparison to vacuum), and many of the char-

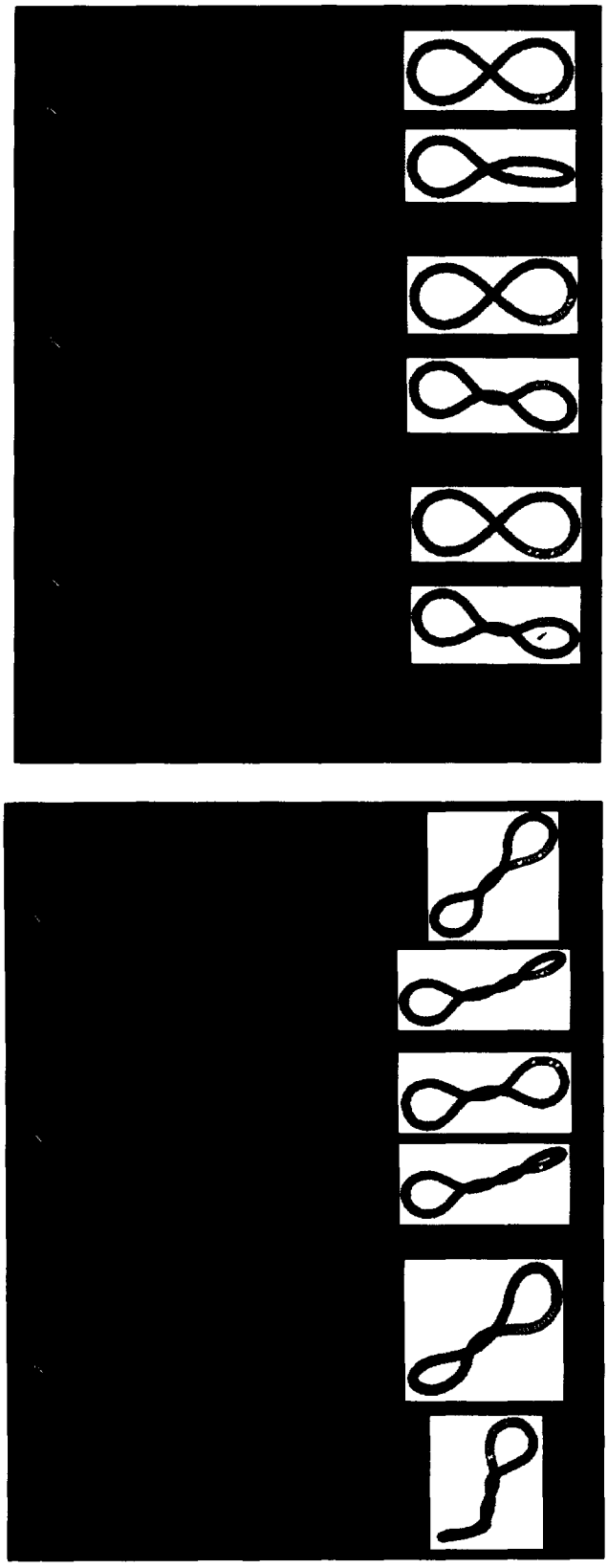

FIGURE 7 Curvature variations along the DNA for the $F1$ and $F2$ families, 1000 bp. The curvature κ at each curve point (112 are used) is plotted for each member of the family ($F1$ or

acteristic harmonic motions are overdamped by solvent.[28] This means that at a given superhelical density, we expect a distribution of forms spanning a *range* of energies and geometries. If we knew those distributions, we could analyze them in terms of the buckling profiles derived from potential energy minimization and understand the "signal vs noise" behavior. This important problem has been the recent focus of Harvey and co-workers.[58]

To estimate such expected distributions, we performed Langevin dynamics simulations at physiological viscosity[28,38] for systems of 1000 bp at various ΔLk (−1, −4, −6) and ρ (3, 1, 0.43). Resulting distributions from trajectories of 60,000 iterations (approximately 600 μs of physical time[38]) are displayed in Figure 10. In each case, we started the simulation at the lowest potential energy minimum identified (see profiles). The thick line in Figure 10 corresponds to $\rho = 1$ ($C = 1.28 \times 10^{-19}$ erg cm); the dashed and thin solid lines correspond, respectively, to $\rho = 3$ and $\rho = 0.43$ ($C = 0.43$ and 3.0×10^{-19} erg cm, respectively). These distributions already reveal important distinctions as a function of ρ.

First, for higher $|\Delta Lk|$ (i.e., 4, 6), distributions are sharper than at $|\Delta Lk| = 1$. More peaks emerge at lower $|\Delta Lk|$. Second, the larger $|\Delta Lk|$ is, the more sensitive the distribution is to ρ. This suggests that experimental data may reproduce distributions that are sensitive to ρ for relatively *small* plasmids at *high* superhelical densities. Thus, for $|\Delta Lk| = 6$ ($|\sigma| \sim 0.063$), distributions for $C = 0.43$, 1.28, and $3.0(\times 10^{-19}$ erg cm) center around $Wr = -1$, −3 and −4, respectively, while for smaller ΔLk the distributions shift toward smaller $|Wr|$ values and are broader. The shifts are more pronounced for lower values of ρ (or higher values of C): compare the progression of distributions at fixed C from the top to bottom panels for both the $C = 1.28$ and $C = 3.0$ series, as opposed to the $C = 0.43$ case. For $|\Delta Lk| = 1$, distributions for all ρ span both the circle and the figure-8 structures. However, the distributions for $C = 0.43$ and 1.28 show higher peaks at the circle, as expected from the profiles (see Figures 1, 3, 4, and 9). Interestingly, the $C = 3.0$ profile spans three configurations: circles, bent circles, and figure-8 like structures.

These distributions tie well with the minimization profiles. For example, the $|Wr|$ vs $|\Delta Lk|$ plot of Figure 1a reveals two local minima at $\Delta Lk = -4$, with $Wr = 0$ and $Wr \sim -1$ (cf. peaks in distribution for $C = 0.43$, shown in middle panel), and no imperfect circle (dip in distribution). It is interesting that for $\Delta Lk = -6$ ($C = 0.43$) structures with writhe near −2 (minor peak) correspond to global minimum but the writhe distribution clusters near the figure-8 family. This is consistent with our finding of the *entropic lowering* of the writhe.[21,28]

For $C = 1.28$ ($\rho = 1$), the distribution for $\Delta Lk = -6$ is again consistent with this lowering tendency, as forms associated with the $F2$ family are preferred over the $F3$. Similarly, for $\Delta Lk = -4$ and −1 the asymmetric distributions indicate a preference of more open, loosely coiled forms than those associated with the potential-energy minimum.

For $C = 3.0$ or $\rho = 0.43$ (see Figure 4a), the sharp distribution near $Wr = -4$ for $\Delta Lk = -6$ corresponds to the actual potential energy minimum identified, but for $\Delta Lk = -4$, the preferred writhe is around −2.5 rather than about −3, indicating again a trend toward more open interwound structures. For this lowest ρ (highest C) examined, all three forms—planar circle, nonplanar circle, and figure-8 interwound—are very close in energy at $\Delta Lk = -1$ (see Figure 4b), and indeed the trimodal distribution displayed in the lower panel of Figure 10 is consistent with the minimization profile.

Phase Diagrams of C/A vs $|\Delta Lk|$

In Figure 11 we present a phase space diagram that delineates the areas where various families are energetically favored as a function of both $C/A(1/\rho)$ and $|\Delta Lk|$. This phase space diagram is motivated by and contains data extracted from that presented by Jülicher.[16] In his analytical treatment of supercoiled DNA using a simple elastic energy model, Jülicher predicted the areas where circles, nonplanar circles, figure-8 forms, and interwound configurations are energetically favored. These regions are identified here by the symbols $F0$, NP, $F1$, and FN, respectively. In addition, Jülicher uses dotted and solid lines to distinguish among the continuous and discontinuous transitions between structures.[16]

$F2$) for $\rho = 3$, 1 and 0.43. The curvature curves corresponding to the first and last structures in the family are superimposed. To the right of the plot, two color configurations are displayed: the upper image corresponds to the beginning of the family (curve of smaller curvature) and the lower to the last structure in the family (curve of greater curvature). The color scheme used for the DNA points on the displayed configurations is color-coded to match that used in the curvature curves.

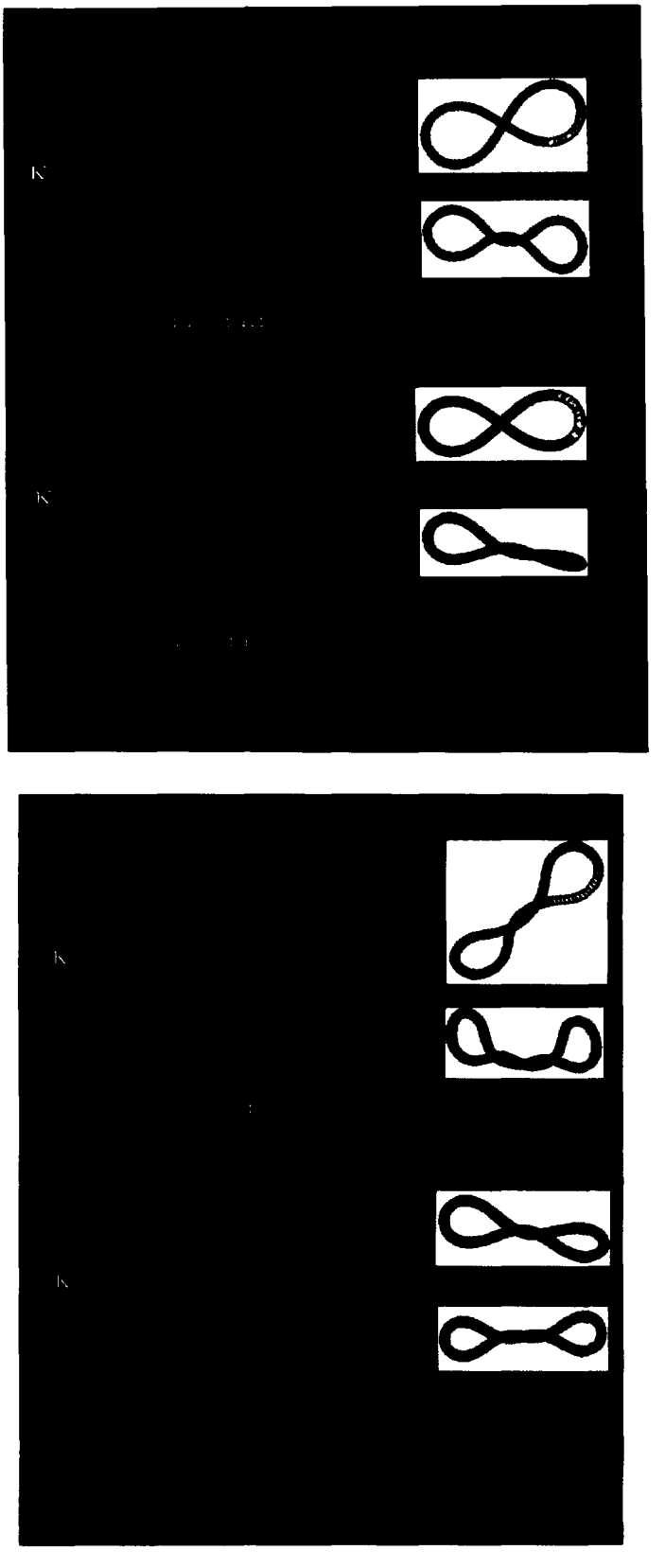

FIGURE 8 Curvature variations along the DNA for the $F1$ and $F2$ families, 1000 bp vs 2000 bp. The curvature κ at each curve point (112 used for the DNA of 1000 bp, 160 for the DNA of 2000 bp) is plotted for the first and last members of the family ($F1$ or $F2$) for $\rho = 0.71$. See Figure 7 caption.

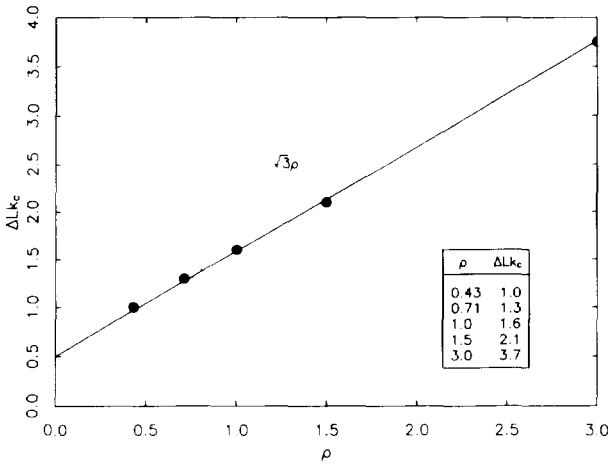

FIGURE 9 The critical value ΔLk_c where the circle and figure-8 forms are energetically equivalent. The value ΔLk_c is obtained from our profiles (Figures 1–4). The value at $\rho = 1.5$ is taken from Ref. 22. The solid line is described by Eq. (5), with the values of the constants ϵ_B and ϵ_t as given in the text. The dots define the "stability" line, $\sqrt{3}\rho$, mentioned in the text.

Our data is shown on the same plot as several points corresponding to the critical values of $|\Delta Lk|$, $|\Delta Lk_c|$, at which two configurational families are energetically equivalent: triangles (Δ) for $NP \rightarrow F0$, open circles ($\circ$) for $NP \rightarrow F1$, plus signs ($+$) for $F0 \rightarrow F1$, and open stars for $F1 \rightarrow F2$ transitions. Two interesting conclusions emerge: (1) Theory and numerical data agree closely for the $NP \rightarrow F0$ and $F0 \rightarrow F1$ transitions, i.e., where self-contact is not important. This can be seen from the close agreement of our triangular, open circular, and plus symbols with the analytical curves. (2) Theory and numerical data depart, as expected, when $|Wr| > 1$, i.e., for structures with more than one point of contact. In particular, our boundary separating $F1$ from $F2$ is shifted significantly to a higher $|\Delta Lk|$ for the corresponding ρ value (e.g., for $\rho = 1$, transition occurs for $\Delta Lk = \pm 2.5$ rather than ± 2.0). Thus, numerical simulations form an important complement to theoretical analysis and an essential tool for treating real DNA. Note also that in the phase space diagram, Jülicher predicts that the nonplanar circle is stable at $\rho \approx 0.61$ ($C/A = 1.64$). From a series of minimizations of the figure-8 at values of ΔLk near -1, we found that indeed this family emerges around $\rho = 0.6$ (see next section).

SUMMARY AND DISCUSSION

In this work we have examined, by energy minimization and Langevin dynamics techniques, the buckling transitions expected from an elastic material with homogeneous bending and twisting and repulsive nonbonded interactions. Our focus was the sensitivity of these results to the ratio of bending to torsional-rigidity constants, $\rho = A/C$. For this reason, the high salt concentration of 1.0M sodium was used. The relevance of these findings to closed circular DNA in solution was explored through examination of the size dependence of buckling transitions as well as the effects of thermal fluctuations. The latter results, presented as writhe distributions as a function of superhelical density and ρ, are consistent with the minimization profiles and also help clarify the dependence on ρ. It is intriguing to explore the possibility that these distributions might be compared to those generated experimentally by a technique that can directly measure the writhe of a plasmid (e.g., cryo-electron microscopy) to help to bracket the biological range of ρ.

Our major findings can be summarized as follows.

Writhe Profiles and Buckling Transitions Are Very Sensitive to ρ

At large ρ, few and distinct families of DNA configurations are expected (Figure 1a), and the buckling transitions among those are both abrupt and large in terms of the spatial change. At small ρ, many smoothly related families emerge (Figure 4a), and larger $|Wr|$ values occur at lower ρ. In particular, the slope of the line $|Wr| \sim 0.72|\Delta Lk|$ obtained from analysis of a few experimental structures (under assumptions of regular interwound structures)[59] corresponds approximately to our results with $\rho = 0.71$.

Further, the family of nonplanar rings expected at low ρ suggests that at sufficiently small values of ρ the first buckling transition (circle to figure-8 form) will already be unobservable, even for very small DNA circles. This is also an interesting hypothesis to test by experiment. On the other hand, we predict that for high ρ buckling might be observable for small DNA circles or loops. In general, we find that the critical $|\Delta Lk|$, ΔLk_c, where the circle and the figure-8 interwound are energetically equivalent, decreases linearly with ρ (Figure 9); this line lies below the stability line $\Delta Lk = \sqrt{3}\rho$ for $\rho > 0.8$, which makes physical sense. Indeed, Jülicher's analysis suggests that this stability line is relevant only for $\rho > 0.6$.[16]

The overall sensitivity of DNA configurations to the ratio of the elastic constants can be seen from

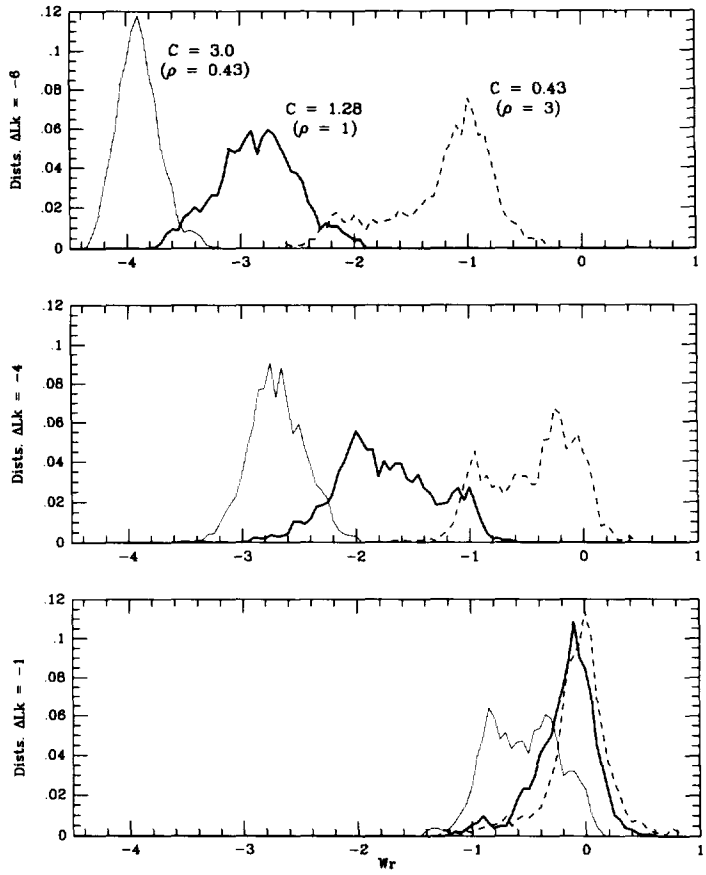

FIGURE 10 Writhe distributions from Langevin dynamics simulations of closed circular DNA, 1000 bp. Shown are writhe distributions for three different values of ΔLk: -1, -4, and -6 (bottom, middle, and top panels) at three different values of ρ—3, 1, 0.43—identified by dashed, thick solid, and thin solid lines, respectively. These three ρ values correspond to $C = 0.43 \times 10^{-19}$ erg cm, 1.28×10^{-19} erg cm, and 3.0×10^{-19} erg cm, respectively, and are labeled in the top panel in units of 10^{-19} erg cm. The distributions are obtained from Langevin dynamics trajectories of length 60,000 iterations (approximately 600 μs). Each such trajectory is started at the lowest energy structure found for the associated values of ΔLk and ρ. The simulations are performed at 1.0 M salt concentration and room temperature conditions, with a Langevin model that incorporates solvent damping effects as described separately.[28]

Figures 12a and 13a. Here, we show the $|Wr|$ value corresponding to minimized structures of 1000 bp as a function of ρ for several values of $|\Delta Lk|$: 0.5, 0.98, 1.5, 2.5, and 5.5. These values of ΔLk were chosen to explore representatives of different families. Clearly, the range of ρ illustrated here (0.1–10; note the logarithmic scale in the abscissa) is large but useful for extended analysis and for other elastic materials. These views might also be relevant to DNA when changes in the chemical environment lead to changes in the elastic constants. To clarify the issues mentioned earlier with respect to the effective persistence length (see section on the ratio of elastic constants under Numerical Model), we generated these views for two values of A in our model: 1.28 and 2.3×10^{-19} erg cm (Figures 12 and 13, respectively). Results are overall very similar and reinforce the point that minima are sensitive to the ratio A/C rather than to the specific values of A or C.

We note from Figures 12a and 13a that each curve (associated with a different ΔLk) decreases monotonically with increasing ρ, with sharp decreases at certain values of ρ, indicating a structural transition. A larger range of $|Wr|$ over the two orders of magnitude of ρ examined here is noted for higher superhelical densities, with this range becoming smaller as $|\Delta Lk|$ decreases. When ρ is small, twisting is penalized more severely, so $|Wr|$ is large relative to $|\Delta Lk|$, i.e., $Wr \sim \Delta Lk$. As ρ increases, the partitioning of superhelicity between twist and writhe changes steadily until a critical

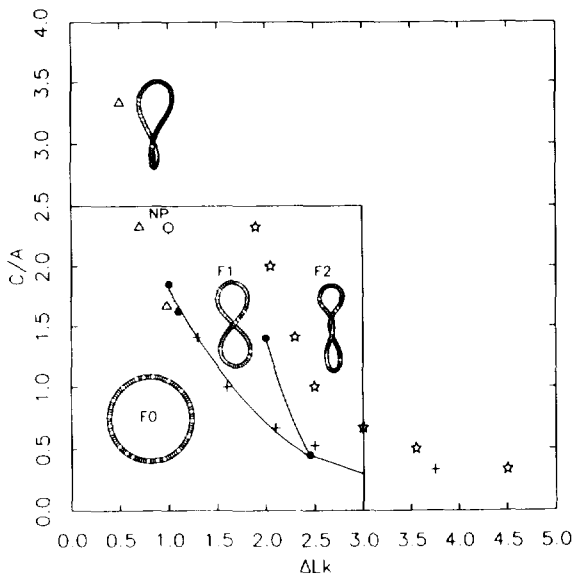

FIGURE 11 A phase diagram (collective profile description) showing behavior for C/A vs $|\Delta Lk|$. The data from Jülicher[16] are shown for comparison with our results. Specifically, the inner box delineates the boundary of Jülicher's reported results. The symbols $F0$, NP, $F1$, and $F2$ separate regions where circles, nonplanar rings, figure-8 forms, and interwound structures, respectively, are energetically favored.[16] The solid circles are critical points, and the solid and dotted curves denote discontinuous and continuous transitions between forms.[16] Our results regarding the critical $|\Delta Lk|$ at which two families are energetically equivalent are overlaid for the following configurational transitions: $F0$ to nonplanar rings (Δ), nonplanar rings to $F1$ forms ($\bigcirc$), $F0$ to $F1$ forms (+), and $F1$ to $F2$ forms (open stars).

value of ρ is reached, at which point a sharp transition to a more open form (different configurational family) results. For $\Delta Lk = -5.5$ at least two such jumps can be seen; the first near $\rho = 1$ is smoother than the second (near $\rho = 5$), which reaches the figure-8 interwound. For $\Delta Lk = -2.5$, the two drops in $|Wr|$ as ρ increases reflect transitions from interwounds with $|Wr| \approx 2$ to structures with $|Wr| \approx 1$ (near $\rho = 1$) and from figure-8 to circle forms (near $\rho = 8$). Overall, we note that, as in the minimization profiles, transitions are sharper for $\rho > 1$. Significantly, substantial differences in $|Wr|$ are observed in the biological range of ρ (say 0.5–1.5). This again suggests that experimental data together with theory might help bracket the relevant ρ range for supercoiled DNA.

In Figures 12b and 13b we plot the energy difference between the circle and the configurations identified in Figures 12a and 13a. The similarity between Figures 12b and 13b is striking. Clearly, the ρ value where the energy difference is zero decreases with decreasing $|\Delta Lk|$. This means that at larger $|\Delta Lk|$ more (interwound) forms are energetically preferred in comparison to the circle. In other words, buckling from the circle occurs for smaller $|\Delta Lk|$ when ρ is smaller. The more pronounced energy jumps at larger ρ are also evident from the figure.

In addition to clarifying the trends presented in this paper, the views of Figures 12 and 13 might have an interesting biological implication. It has been suggested by Schurr and co-workers that changes in the secondary structure of DNA occur as superhelical stress increases.[56] These changes would lead to an abrupt alteration of the elastic constants and subsequently a sudden (putting aside thermal fluctuations) change in the three-dimensional shape of the DNA. It is clearly inappropriate to interpret changes in secondary structure on the basis of simulations involving a homogeneous model unless the transition would be homogeneous in some sense, but analogous data might be generated for an inhomogeneous model. Our data indicate, in particular, that the first transition is most sensitive to ρ, so an experimental following of DNA at low superhelical densities as physiological density is approached might exhibit the most pronounced behavior. This is consistent with the observations of Song et al. by fluorescence polarization anisotropy measurements.[56]

Buckling Transitions Are Masked as DNA Size Increases

Our comparison of buckling profiles for DNA systems of 1000 and 2000 bp (Figures 3 and 5) clearly shows that configurational and energetic evolutions as a function of ΔLk vary more smoothly as DNA size increases. These observations can be explained in terms of lower curvature for larger plasmids (Figures 7 and 8). Thus, buckling transitions are expected to be masked for plasmids of biological interest (several thousand bp), except possibly for very large ρ. For DNA minicircles and small loops, however, buckling phenomena, especially the circle to figure-8 transition, might be observable, as already suggested,[57] and might be important in regulatory mechanisms. That is, the biological activity of an enzyme that changes the linking number deficit of topologically constrained DNA might be facilitated by an abrupt configurational change in response to a smooth deformation at a certain range of supercoiling stress.[34,35]

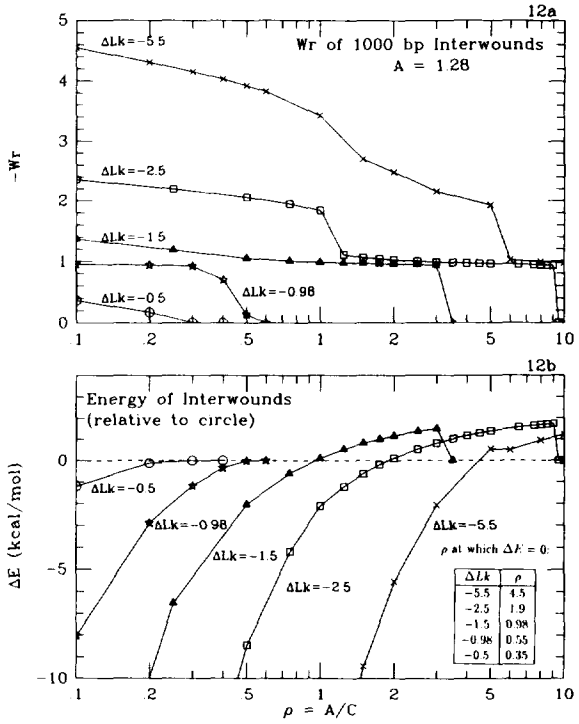

FIGURE 12 Structural transitions of closed circular DNA at fixed ΔLk as a function of ρ: $A = 1.28 \times 10^{-19}$ erg cm. (a) The values $-Wr$ for energy minimized closed-circular DNA of length 1000 bp are shown at fixed ΔLk as ρ (plotted on a logarithmic scale) is varied. The value of A is labeled on the plot in units of 10^{-19} erg cm. (b) The energies of the interwound structures relative to the relaxed circle are plotted as a function of ρ (also on a logarithmic scale). The table inset indicates the values of ρ at which the energy difference between circle and interwound ΔE is zero.

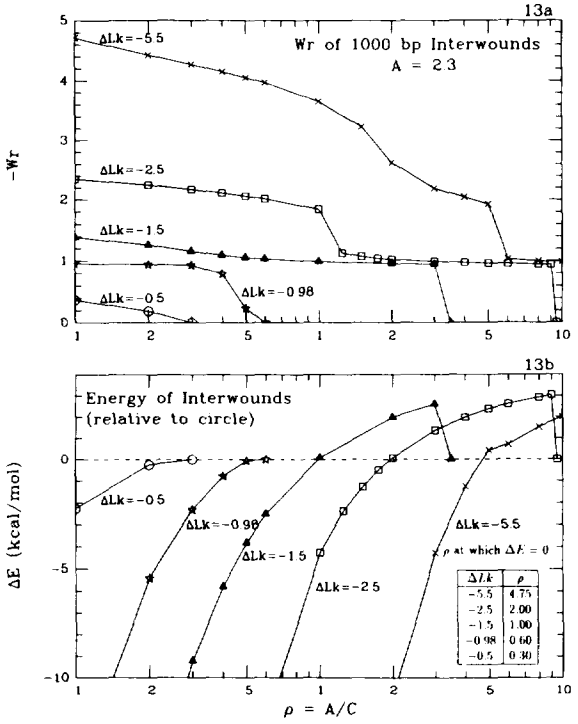

FIGURE 13 Structural transitions of closed circular DNA at fixed ΔLk as a function of ρ: $A = 2.3 \times 10^{-19}$ erg cm. See caption to Figure 12.

Buckling Transitions Are Masked/ Softened by Thermal Fluctuations

Our writhe distributions from dynamic simulations of DNA in solvent indicate that a *range* of configurations and energies is expected at a typical solution environment, rather than a sampling of any one major family identified in the minimization profiles. While this basic result is expected, and also demonstrated by Harvey and co-workers,[58] the quantitative data presented in this connection (Figure 10) also reveal other trends. First, an entropic lowering of the writhe (i.e., a tendency of the DNA to adopt more open forms in comparison to the potential energy minimum) is evident. This tendency is more pronounced for larger ρ and larger $|\Delta Lk|$. Second, the differences among the distributions associated with different ρ are largest for greater superhelical densities. Both the top and middle panels of Figure 10, which correspond to typical superhelical densities, reveal the displacements of the distributions from one another (for different ρ), suggesting that these trends should be experimentally observable. Third, the distribution locations are most sensitive to $|\Delta Lk|$ for smaller ρ; that is, significant shifts in the distribution ranges are more dramatic for smaller ρ. This again suggests that the actual shifts observed in such laboratory-generated distributions might help bracket the prevalent value of ρ.

Phase Diagrams of $|Wr|$ vs ρ Indicate the Importance of Self-Contact Interactions Beyond the $|Wr| = 1$ Structure and Hence the Complement of Theory and Numerical Work

We found from the analysis of Figure 11 that predictions from an analytical treatment of the DNA as an infinitely thin elastic rod with no self-contact[16] are very accurate for structures with little or no self-contact, i.e., conformations with $|Wr| < 1$. Indeed, our numerical results from a model that includes self-contact agree very closely with those of Jülicher for transitions between the circle, nonplanar circle, and figure-8 families.[16] The theoretical work of Jülicher, moreover, can predict the

stability of the various configurations,[16] an issue not straightforward to address by our potential-energy minimization approach. However, in the case of highly writhed structures, self-contact becomes critically important, and analytical treatments must be complemented with numerical work that can easily model nonbonded, electrostatic potentials more realistically. Our comparison with the analytic phase diagram, in particular, shows a pronounced shift in the line delineating the $F1$ and $F2$ interwound regions (Figure 11).

Possible Application to DNA's Torsional Stiffness

It is interesting to explore how the results summarized above might be applied. Essentially, our data present a collective picture of a very stiff DNA at large ρ values. In this regime, the DNA tends to cluster around a rather small set of structures that are similar in writhe for a rather large range of ΔLk until some critical threshold of superhelical stress is reached, at which point there occurs an abrupt transition from one DNA structure into another (Figures 1a and 10). At the other extreme, when $\rho \ll 1$, a very large difference in Wr as ΔLk increases (see Figure 4a for $\rho = 0.43$) is noted. Thus, at very low values of A/C, the DNA is much more flexible and can easily move from one writhe structure to another with a small change in superhelical stress. While thermal fluctuations mask specific structural transitions, differences in writhe corresponding to accessible DNA configurations at a given (fixed) ΔLk still exist. Figure 10 shows that such differences are pronounced at higher ΔLk, in fact around values of physiological superhelical densities. Writhe variances are expected to increase with size[60] but might be quite useful in practice for DNA systems of 1000 bp or smaller.

Based on the above findings, a possible application arises concerning the torsional stiffness. As discussed in the introduction, uncertainty exists regarding the relevant value of C.[43-45,49,51,56,61] Indeed, there have been extensive discussions in the literature regarding the dependence of thermal fluctuations on the elastic constants and interpretation of this dependence in terms of various polymer models and experimental data. One procedure that has been used to estimate C was first described by Benham,[47] explored by Vologodskii et al.[48] and later refined by Klenin et al.,[46] who also accounted for excluded volume, and arrived at the value $C = 3 \times 10^{-19}$ erg cm. This technique estimates C from the variance in twist in nicked DNA molecules as a difference of two terms: an experimentally measured variance in ΔLk (reflecting equilibrium fluctuations) and a numerically derived variance in writhe:

$$\langle (\Delta Tw)^2 \rangle = \langle (\Delta Lk)^2 \rangle - \langle (Wr)^2 \rangle = \left(\frac{L}{4\pi^2}\right)\frac{k_B T}{C} \quad (8)$$

Indeed, many theorists have studied the generation of writhe moments on the basis of various polymer models[62-64]; see chapter IIA of Ref. 60 for a summary.

The above relation assumes statistical independence of the writhe and twist fluctuations, i.e., $Cov(\Delta Tw, Wr) = 0$. While it is possible that this term is smaller in magnitude than the variances in writhe and twist, it is not known by how much and how its magnitude might affect estimates of the torsional stiffness (see discussions of Benham[65] and Shore and Baldwin,[44] for example).

Now that experimental techniques are permitting improved imaging of DNA,[4,6,66] including direct measurements of the writhe,[67] perhaps a slightly different approach might be considered. Rather than relying on theoretically derived writhe variances for nicked DNA, a series of writhe distributions for various ρ values might be considered and compared to writhe distributions derived by extensive imaging experiments.

Observing the writhe distribution of DNA plasmids (at a given ΔLk) in solution without change of structure due to the imaging process is not a trivial task. The reliability of this technique, however, is likely to increase in the coming years. Techniques in this class include cryo-electron microscopy[66] and SFM.[4] Both have received increased attention recently and have been used to explore many interesting properties of DNA.

The experiment might be used to produce writhe distributions of a specific mixed-sequence DNA plasmid at a series of superhelical densities, and these could be compared to numerical data such as shown in Figure 10. However, it is not clear that the biological regime of ρ will be sufficient to produce sensitive patterns. Furthermore, because of the expected sharp increase of writhe variance with size, the plasmid should be as small as possible, 500–1000 bp. From studies of nicked DNA, a sharp variance in writhe is noted around 1000 bp,[46] so the writhe fluctuations should be easier to describe below this size where thermal fluctuations are much smaller. High salt conditions, as used here, would probably result in more discernible patterns, and other special experimental techniques

(changes in the environment) might be developed to make measurements as sensitive as possible. A procedure to determine *Wr* from the direct images will also have to be perfected (e.g., Ref. 67) and, furthermore, the flat (rather than three-dimensional) origin of the configurations considered (i.e., perhaps by computing analogous distributions to those shown in Figure 10 for projected plasmids). Clearly, it is not known if the resolution of experiment will be sufficiently good for this purpose and, in any case, a large amount of reliable data will have to be generated before experimental distributions can be constructed.

We hope further synergy will be possible between experiment and modeling with respect to supercoiled DNA. Direct imaging techniques are steadily improving,[4,5] and advances in both computer hardware and software are increasing the reliability and accuracy of simulation results. Certainly, the elastic model approximation has been useful for a long time, but finer resolutions of nucleic acid models will undoubtedly be pursued in the coming years to permit studies on new levels. The most recent improvements in treating the long-range electrostatic interactions in atomic-resolution DNA simulations,[68,69] for example, will undoubtedly considerably increase the quality of all-atom nucleic acid simulations. A possible merging of the macroscopic with the microscopic treatments for DNA can be anticipated in the coming years.

This work is supported by the National Institutes of Health (Research Resource RR08102) and an Alfred P. Sloan fellowship. Computational resources were provided in part by the Cornell Theory Center. We thank Drs. Jerry Manning, Wilma Olson, and Alex Vologodskii for valuable comments. We are grateful to Hongmei Jian for related simulation work regarding the influence of the Debye-Hückel potential on the effective persistence length. TS is an investigator of the Howard Hughes Medical Institute.

REFERENCES

1. White, J. H. (1989) in *Mathematical Methods for DNA Sequences*, Waterman, M. S., Ed., CRC Press, Boca Raton, FL, Chap. 9.
2. Cozzarelli, N. R. & Wang, J. C., Eds. (1990) *DNA Topology and Its Biological Effects*. Cold Spring Harbor Laboratory Press, Cold Spring Harbor, NY.
3. Brady, G. W., Fein, D. B., Lambertson, J., Grassian, V., Foos, D. & Benham, C. J. (1983) *Proc. Natl. Acad. Sci. USA* **80,** 741.
4. Samori, B., Nigro, C., Armentano, V., Cimieri, S., Zuccheri, G. & Quagliariello, C. (1993) *Angew. Chem. Int. Ed. Engl.* **32,** 1461.
5. Bustamante, C., Erie, D. A. & Keller, D. (1994) *Curr. Opin. Struct. Biol.* **4,** 750.
6. Adrian, M., Bordier, B. H., Wahli, W., Stasiak, A. Z., Stasiak, A. & Dubochet, J. (1990) *EMBO J.* **9,** 4551.
7. Zhurkin, V. B., Lysov, Y. P. & Ivanov, V. (1979) *Nucleic Acid Res.* **6,** 1081.
8. Tobias, I. & Olson, W. K. (1993) *Biopolymers* **33,** 639.
9. Dichmann, D. J., Li, Y. & Maddocks, J. H. (1996) in *Mathematical Applications to Biomolecular Structure and Dynamics, IMA Volumes in Mathematics and its Applications*, Vol. 82, Mesirov, J. P., Schulten K. & Sumners, D. W., Eds., Springer-Verlag, New York, pp 71-113.
10. Hearst, J. E. & Hunt, N. G. (1991) *J. Chem. Phys.* **95,** 9322.
11. Hunt, N. G. & Hearst, J. E. (1991) *J. Chem. Phys.* **95,** 9329.
12. Shi, Y. & Hearst, J. E. (1994) *J. Chem. Phys.* **101,** 5186.
13. Le Bret, M. (1979) *Biopolymers* **18,** 1709.
14. Benham, C. J. (1989) *Phys. Rev. A* **39,** 2852 (1989).
15. Le Bret, M. (1984) *Biopolymers* **23,** 1835.
16. Jülicher, F. (1994) *Phys. Rev. E* **49,** 2429.
17. Lahiri, A. (1994) *Biopolymers* **34,** 799.
18. Marko, J. F. & Siggia, E. D. (1994) *Science* **265,** 506.
19. Hao, M.-H. & Olson, W. K. (1989) *Biopolymers* **28,** 873.
20. Hao, M.-H. & Olson, W. K. (1989) *Macromolecules* **22,** 3292.
21. Schlick, T. & Olson, W. K. (1992) *J. Mol. Biol.* **223,** 1089.
22. Schlick, T., Li, B. & Olson, W. K. (1994) *Biophys. J.* **67,** 2146.
23. Liu, G., Olson, W. K. & Schlick, T. (1995) *Comp. Polym. Sci.* **5,** 7.
24. Yang, Y., Tobias, I. & Olson, W. K. (1993) *J. Chem. Phys.* **98,** 1673.
25. Bauer, W. R., Lund, R. A. & White, J. H. (1993) *Proc. Natl. Acad. Sci. USA* **90,** 833.
26. Vologodskii, A. V. & Cozzarelli, N. R. (1994) *Ann. Rev. Biophys. Biomol. Struct.* **23,** 609.
27. Tan, R. K. Z. & Harvey, S. C. (1989) *J. Mol. Biol.* **205,** 573.
28. Ramachandran, G. & Schlick, T. (1995) *Phys. Rev. E* **51,** 6188.
29. Chirico, G. & Langowski, J. (1994) *Biopolymers* **34,** 415.
30. Klapper, I. (1996) *J. Comp. Phys.*, **125,** 325.
31. Schlick, T. (1995) *Curr. Opin. Struc. Biol.* **5,** 245.
32. Schlick, T., Olson, W. K., Westcott, T. & Greenberg, J. P. (1994) *Biopolymers* **34,** 565.
33. Zajac, E. E. (1962) *Trans. ASME Ser. E J. Appl. Mech.* **29,** 136.
34. Zhang, P., Tobias, I. & Olson, W. K. (1994) *J. Mol. Biol.* **242,** 271.

35. Tobias, I., Coleman, B. & Olson, W. K. (1994) *J. Chem. Phys.* **101,** 10990.
36. Schlick, T., Hingerty, B. E., Peskin, C. S., Overton, M. L. & Broyde, S. (1991) in *Theoretical Biochemistry and Molecular Biophysics*, Vol. 1, Beveridge, D. L. & Lavery, R., Eds., Adenine Press, Schenectady, NY, pp. 39–58.
37. Peskin, C. S. & Schlick, T. (1989) *Comm. Pure App. Math.* **42,** 1001.
38. Ramachandran, G. & Schlick, T. (1996) in *Global Minimization of Non-Covex Energy Functions: Molecular Conformation and Protein Folding* (DIMACS Series in Discrete Mathematics and Theoretical Computer Science, Vol. 23), American Mathematical Society, Providence, RI, pp. 215-231.
39. Zhang, G. & Schlick, T. (1993) *J. Comp. Chem.* **14,** 1212.
40. Schlick, T., Li, B. & Hao, M.-H. (1994) in *Structural Biology: State of the Art 1993, Proceedings of the Eighth Conversations, Volume 1*, Sarma, R. & Sarma, M., Eds., Adenine Press, Schenectady, NY, pp. 157–174.
41. Hagerman, P. J. (1988) *Ann. Rev. Biophys. Biophys. Chem.* **17,** 265.
42. Barkley, M. D. & Zimm, B. H. (1979) *J. Chem. Phys.* **70,** 2991.
43. Shore, D. & Baldwin, R. L. (1983) *J. Mol. Biol.* **170,** 957.
44. Shore, D. & Baldwin, R. L. (1983) *J. Mol. Biol.* **170,** 983.
45. Horowitz, D. S. & Wang, J. C. (1984) *J. Mol. Biol.* **173,** 75.
46. Klenin, K. V., Vologodskii, A. V., Anshelevich, V. V., Klisko, V. Y., Dykhne, A. M. & Frank-Kamenetskii, M. D. (1989) *J. Biomol. Struct. Dynam.* **6,** 707.
47. Benham, C. J. (1978) *J. Mol. Biol.* **123,** 361.
48. Vologodskii, A. V., Anshelevich, V. V., Lukashin, A. V. & Frank-Kamenetskii, M. D. (1979) *Nature* **280,** 294.
49. Clendenning, J. B., Naimushin, A. N., Fujimoto, B. S., Stewart, D. W. & Schurr, J. M. (1994) *Biophys. Chem.* **52,** 191.
50. Gebe, J. A., Allison, S. A., Clendenning, J. B. & Schurr, J. M. (1995) *Biophys. J.* **68,** 619.
51. Millar, D. P., Robbins, R. J. & Zewail, A. H. (1982) *J. Chem. Phys.* **76,** 2080.
52. Gorin, A. A., Zhurkin, V. B. & Olson, W. K. (1995) *J. Mol. Biol.* **247,** 34.
53. Olson, W. K., Babcock, M. S., Gorin, A., Liu, G.-H., Markey, N. L., Martino, J. A., Pedersen, S. C., Srinivasan, A. R., Tobias, I., Westcott, T. P. & Zhang, P. (1995) *Biophys. Chem.* **55,** 7.
54. Manning, G. S. (1981) *Biopolymers* **20,** 1751.
55. Vologodskii, A. V. & Cozzarelli, N. R. (1995) *Biopolymers* **35,** 289.
56. Song, L., Fujimoto, B. S., Wu, P., Thomas, J. C., Shibata, J. H. & Schurr, J. M. (1990) *J. Mol. Biol.* **241,** 307.
57. Bednar, J., Furrer, P., Stasiak, A., Dubochet, J., Engelman, E. H. & Bates, A. D. (1994) *J. Mol. Biol.* **235,** 825.
58. Sprous, D., Tan, R. K.-Z. & Harvey, S. C. (1996) *Biopolymers* **39,**243–258.
59. Boles, T. C., White, J. H. & Cozzarelli, N. R. (1990) *J. Mol. Biol.* **213,** 931.
60. Vologodskii, A. (1992) *Topology and Physics of Circular DNA*, CRC Press, Boca Raton, FL.
61. Naimushin, A. N., Clendenning, J. B., Kim, U., Song, L., Fujimoto, B. S., Stewart, D. W. & Schurr, J. M. (1994) *Biophys. Chem.* **52,** 219.
62. Le Bret, M. (1980) *Biopolymers* **19,** 619.
63. Chen, Y. D. (1981) *J. Chem. Phys.* **75,** 2447.
64. Shimada, J. & Yamakawa, H. (1988) *Biopolymers* **27,** 657.
65. Benham, C. J. (1990) in *Structure and Methods Volume 3: DNA and RNA*, Sarma, R. H. & Sarma, M. H., Eds., Adenine Press, Guilderland, NY, pp. 17–38.
66. Dubochet, J., Adrian, M., Chang, J.-J., Homo, J. C., Lepault, J., McDowall, A. W. & Schultz, P. (1988) *Quart. Rev. Biophys.* **21,** 129.
67. Zuccheri, G., Raneri, G. A., Nigro, C. & Samori, B. (1995) *J. Vac. Sci. Technol. B* **13,** 158.
68. York, D. M., Yang, W., Lee, H., Darden, T. & Pederson, L. G. (1995) *J. Am. Chem. Soc.* **117,** 5001.
69. Cheatham, T. E., III, Miller, J. L., Fox, T., Darden, T. A. & Kollman, P. A. (1995) *J. Am. Chem. Soc.* **117,** 4193.

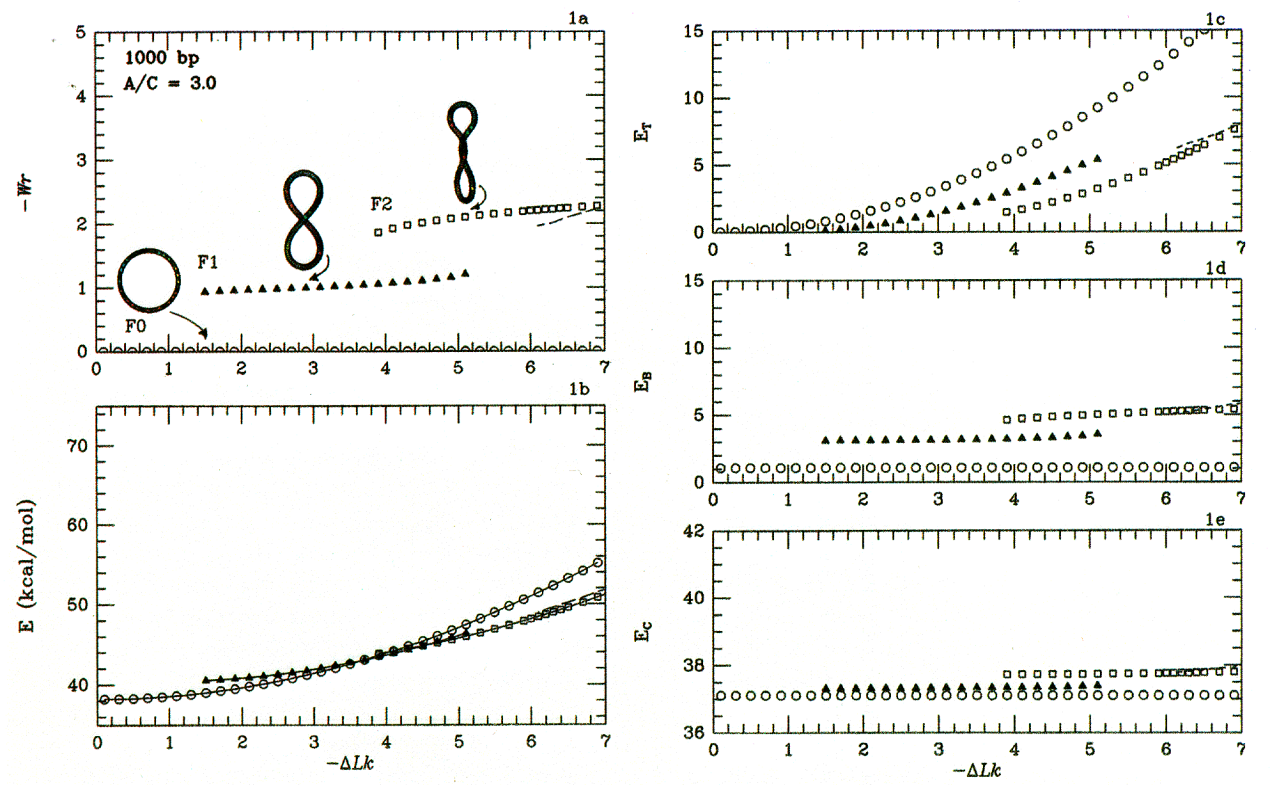

FIGURE 1

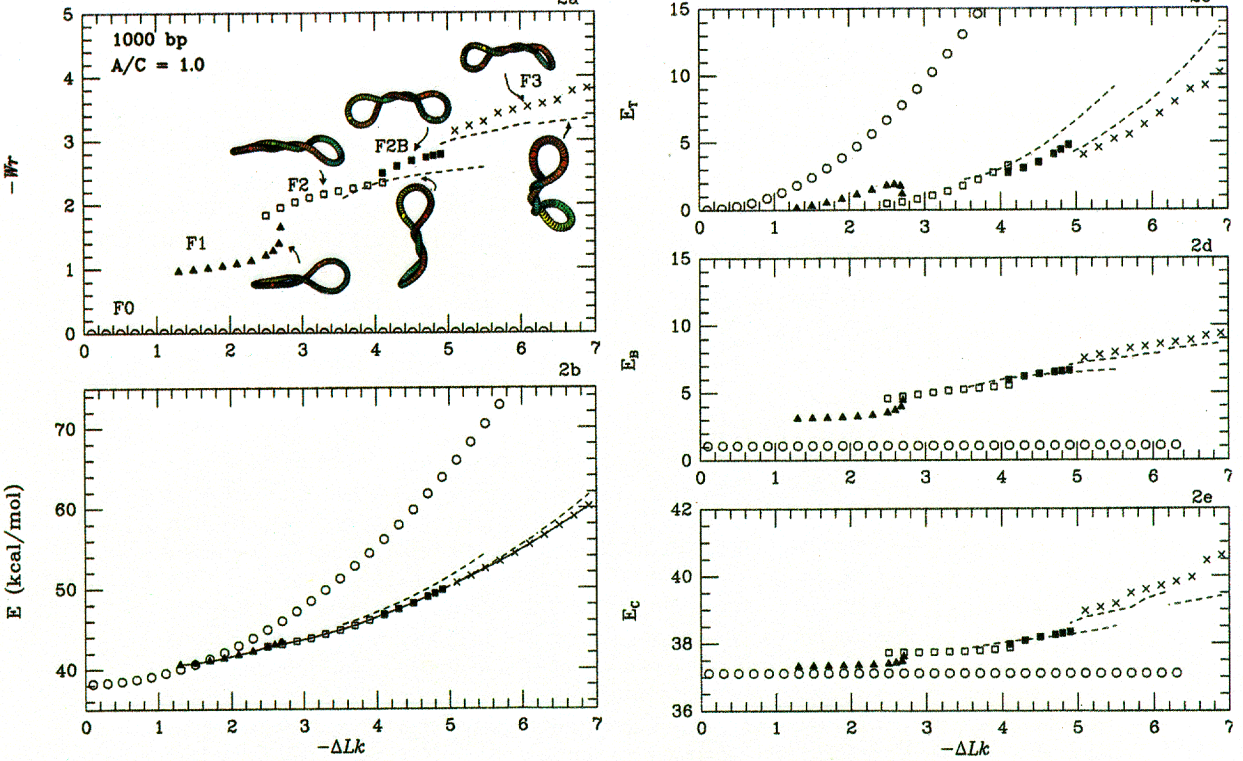

FIGURE 2 Energy-minimized profiles for closed circular DNA of length 1000 base pairs, $\rho = 1$. See Figure 1 caption.

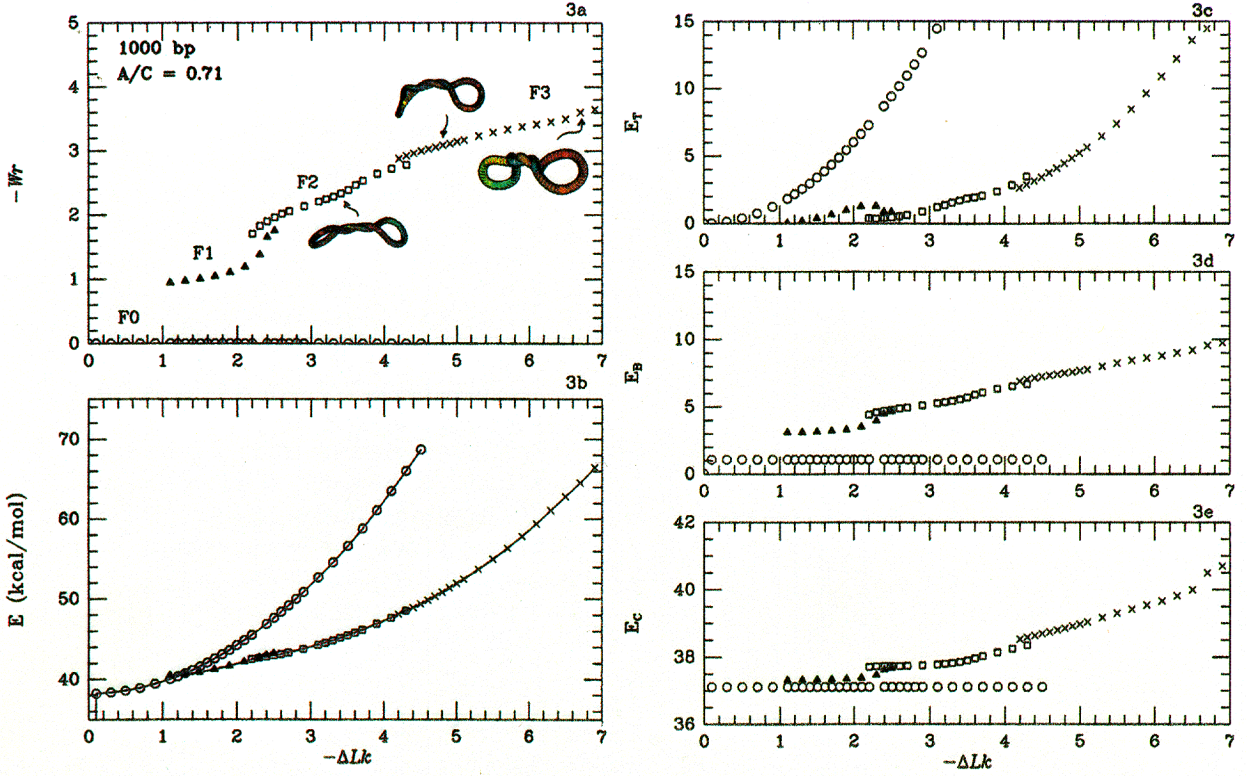

FIGURE 3 Energy-minimized profiles for closed circular DNA of length 1000 base pairs, $\rho = 0.71$. See Figure 1 caption.

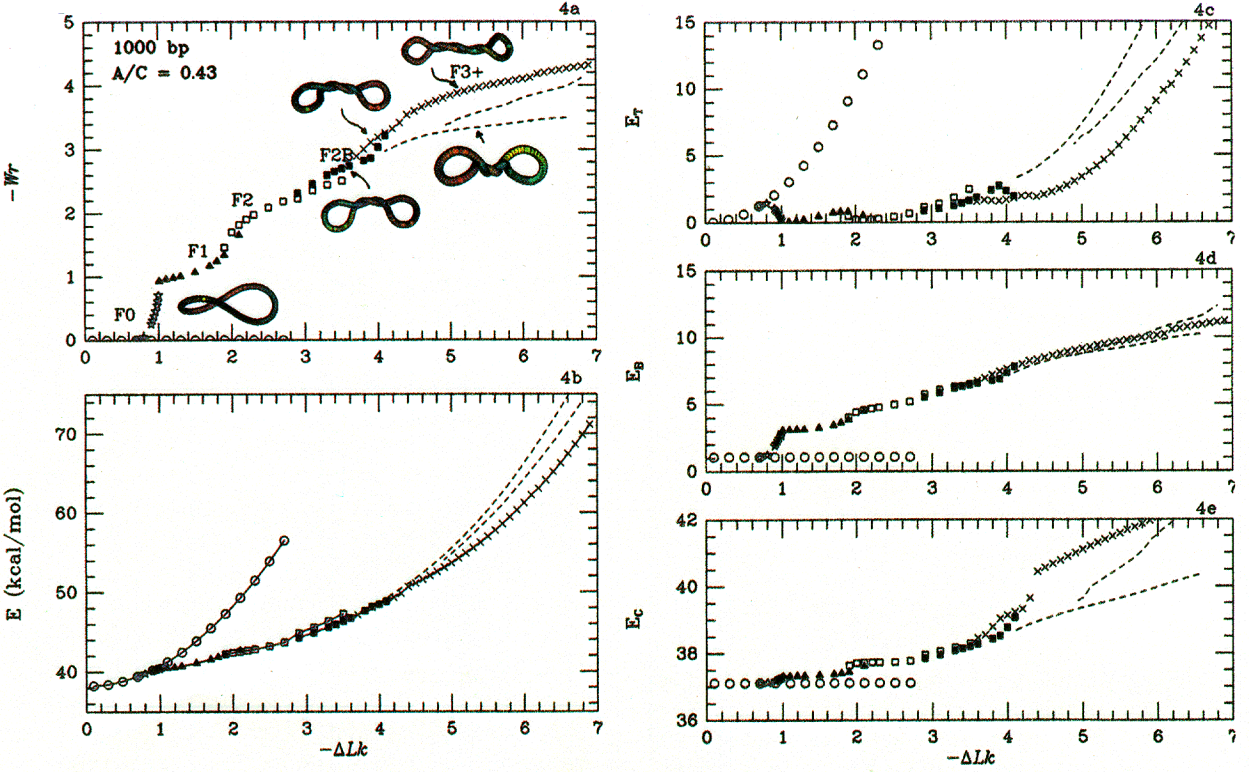

FIGURE 4 Energy-minimized profiles for closed circular DNA of length 1000 base pairs, $\rho = 0.43$. See Figure 1 caption.

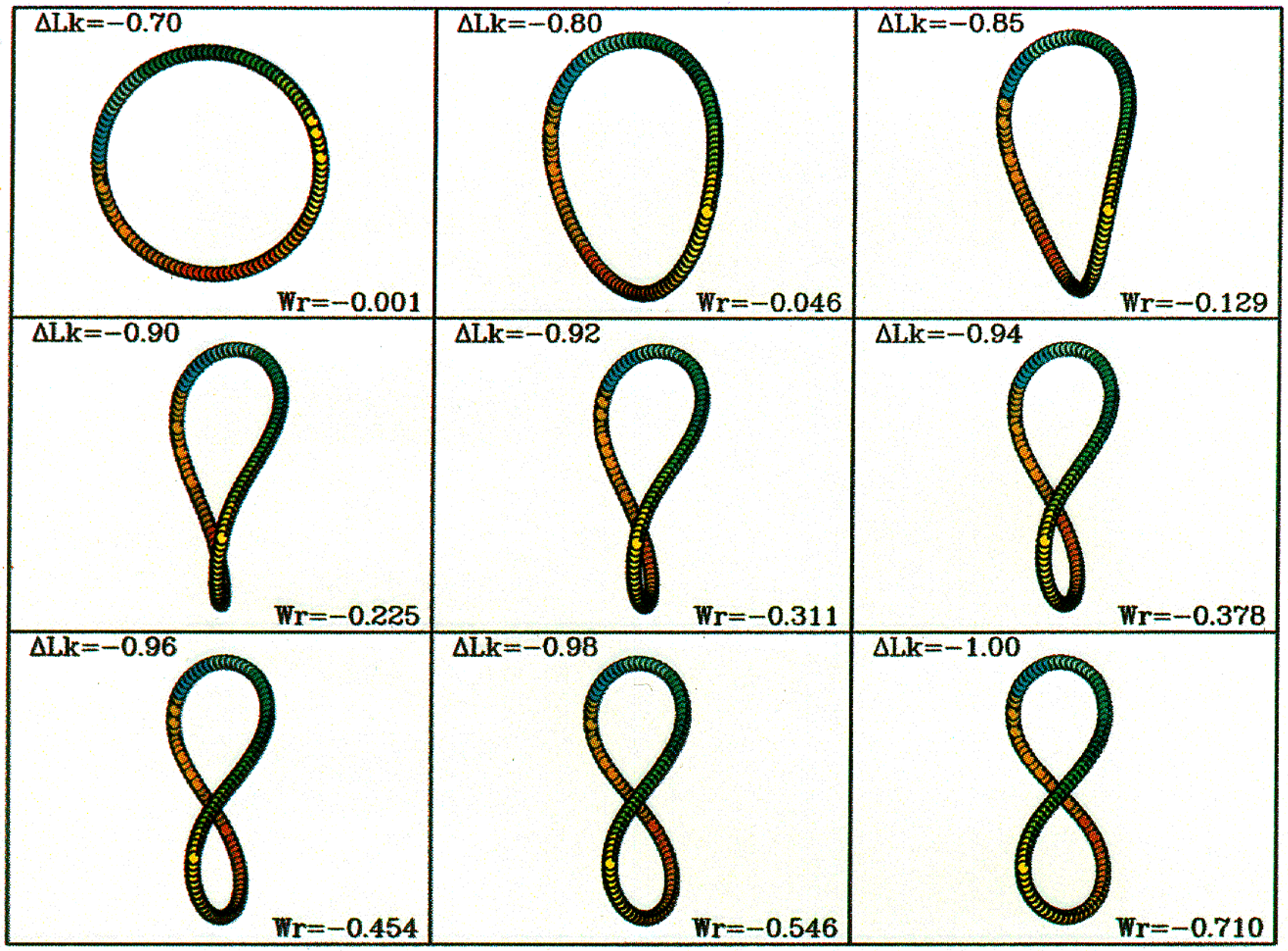

FIGURE 6 The nonplanar-circle family identified at $\rho = 0.43$. These forms correspond to the branch of $0 < |Wr| < 1$ shown in Figure 4a by open star symbols. Note the progression from a slightly bent circle at $-\Delta Lk = 0.7$ to the nearly figure-8 form at $-\Delta Lk = 1.0$.

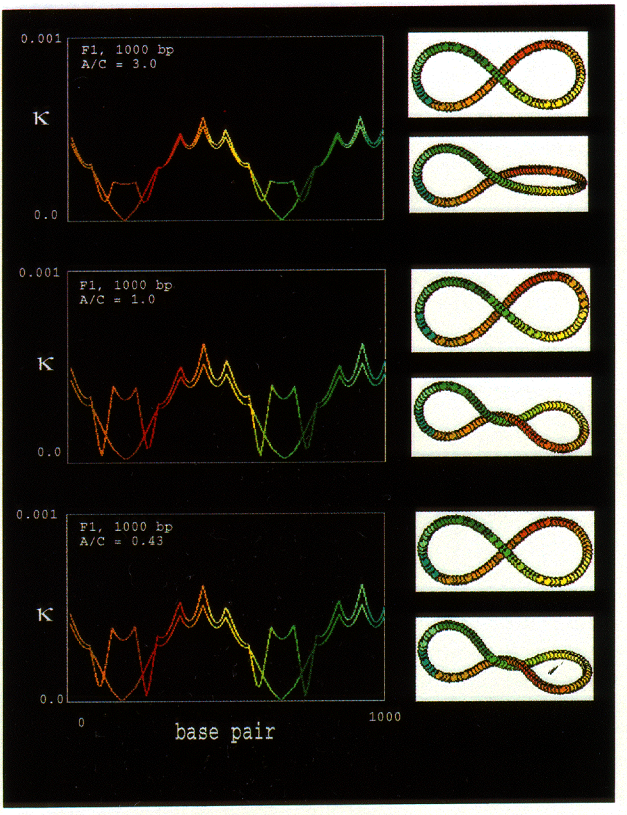

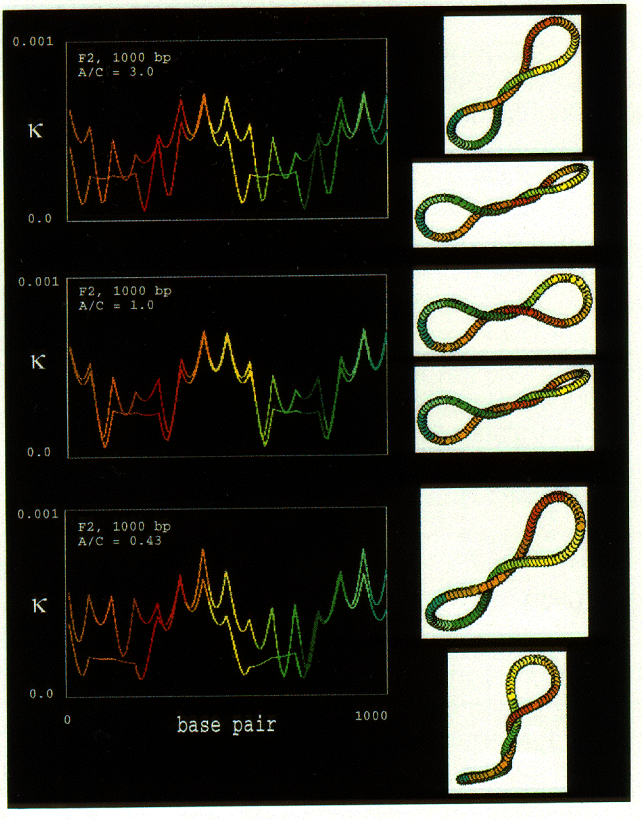

FIGURE 7 Curvature variations along the DNA for the $F1$ and $F2$ families, 1000 bp. The curvature κ at each curve point (112 are used) is plotted for each member of the family ($F1$ or

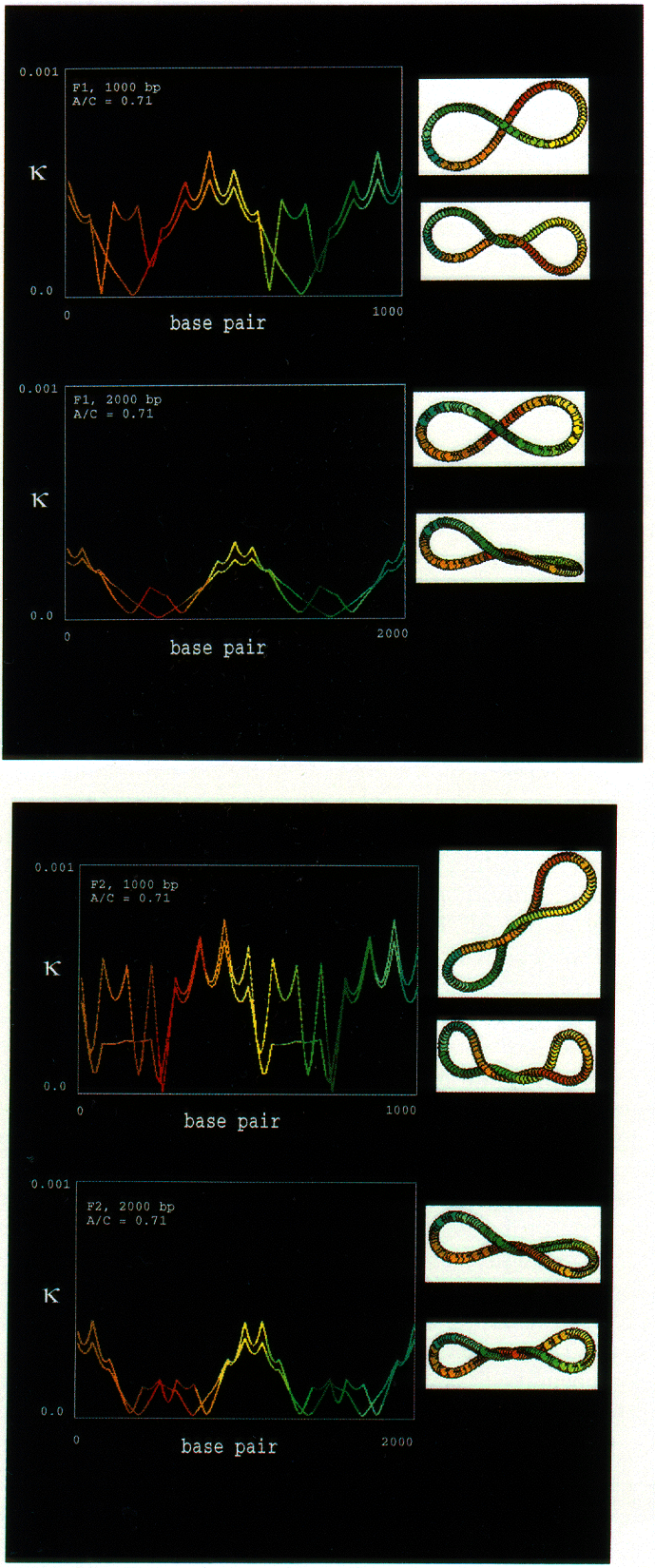

FIGURE 8 Curvature variations along the DNA for the $F1$ and $F2$ families, 1000 bp vs 2000 bp. The curvature κ at each curve point (112 used for the DNA of 1000 bp, 160 for the DNA of 2000 bp) is plotted for the first and last members of the family ($F1$ or $F2$) for $\rho = 0.71$. See Figure 7 caption.